ATRX modulates the escape from a telomere crisis

Helene E. B. Geiller[1], Adam Harvey[2], Rhiannon E. Jones[1], Julia W. Grimstead[1], Kez Cleal[1], Eric A. Hendrickson[2¶] and Duncan M. Baird[1¶*].

[1]Division of Cancer and Genetics, School of Medicine, Cardiff University, Heath Park, Cardiff, United Kingdom

[2]Department of Biochemistry, Molecular Biology, and Biophysics, University of Minnesota Medical School, Minneapolis, Minnesota, USA

[¶]Co-senior authors.

[*]Corresponding author: bairddm@cardiff.ac.uk

Key points:

1. Telomere crisis is required to induce the ALT phenotype in the absence of ATRX

2. ATRX stringently represses the escape from crisis in mesenchymal cells

3. Telomeric mutation is consistent with the addition of sequences via a replicative process

Abstract

Telomerase activity is the principal telomere maintenance mechanism in human cancers, however 15% of cancers utilise a recombination-based mechanism referred to as alternative lengthening of telomeres (ALT) that leads to long and heterogenous telomere length distributions. Loss-of-function mutations in the Alpha Thalassemia/Mental Retardation Syndrome X-Linked (ATRX) gene are frequently found in ALT cancers. Here, we demonstrate that the loss of ATRX, coupled with telomere dysfunction during crisis, is sufficient to initiate activation of the ALT pathway and that it confers replicative immortality in human fibroblasts. Additionally, loss of ATRX combined with a telomere-driven crisis in HCT116 epithelial cancer cells led to the initiation of an ALT-like pathway. In these cells, a rapid and precise telomeric elongation and the induction of C-circles was observed; however, this process was transient and the telomeres ultimately continued to erode such that the cells either died or the escape from crisis was associated with telomerase activation. In both of these instances, telomere sequencing revealed that all alleles, irrespective of whether they were elongated, were enriched in variant repeat types, that appeared to be cell-line specific. Thus, our data show that the loss of ATRX combined with telomere dysfunction during crisis induces the ALT pathway in fibroblasts and enables a transient activation of ALT in epithelial cells.

Author Summary

Telomeres are nucleoprotein structures that cap the ends of linear chromosomes, they are essential for chromosomal stability, but gradually shorten with ongoing cell division. The loss of telomeric DNA ultimately leads to the loss of the end capping function, the induction of widespread genomic instability and cellular crisis. This period of crisis leads to the acquisition of telomere maintenance mechanisms (TMM) that are required to confer replicative immortality in cancer cells. The majority of tumour types use telomerase as their TMM, but a significant subset of cancers utilise the alternative lengthening of telomeres (ALT) pathway. Here we show that, in the absence of the Alpha Thalassemia/Mental Retardation Syndrome X-Linked (ATRX) gene, fibroblast cells, that very rarely escape crisis, can efficiently escape crisis having induced the ALT pathway. In contrast, epithelial cells that escape crisis having activated telomerase, are restricted by the absence of ATRX, but can induce a transient ALT-like activity in a small proportion of cells. Our data point to an important role of ATRX in conferring telomere stability and restricting clonal evolution during a telomere-driven crisis in cells of a mesenchymal origin.

47 **INTRODUCTION**

48 Telomeres are repetitive DNA:protein elements that protect the ends of linear chromosomes and
49 prevent their recognition as double-stranded DNA breaks [1]. As a consequence of the "end-
50 replication problem", telomeres shorten with every successive cell cycle and such shortening
51 ultimately limits the proliferative capacity of cells, by eliciting a TP53-dependent G_1/S cell cycle arrest
52 that acts as a stringent tumour suppressive mechanism [2]. In the absence of a functional cell-cycle
53 arrest, continued cell division and telomere erosion ultimately result in a period of telomere
54 dysfunction, referred to as "crisis" [3]. Telomere dysfunction during crisis leads to large-scale genomic
55 rearrangements from which cells can escape by activating a telomere maintenance mechanism (TMM)
56 that rescues cell viability but drives clonal evolution and tumour progression [4, 5]. The majority of
57 malignancies, as well as stem cells, germ cells and single-celled organisms, almost exclusively utilise
58 the enzyme complex telomerase as their primary TMM [6, 7]. However, 15% of malignancies,
59 predominantly those of mesenchymal origin [8], do not express telomerase, but instead maintain their
60 telomeres via the Alternative Lengthening of Telomeres (ALT) mechanism [9, 10].

61 ALT was originally characterised by extreme telomere length heterogeneity and an absence of
62 telomerase activity [11]. Subsequently, ALT-associated promyelocytic leukaemia (PML) nuclear bodies
63 (APBs) were identified that contain telomeric repeat DNA and the telomere binding proteins telomere
64 repeat factors 1 and 2 (TRF1 and TRF2), associated with the PML protein [12]. APBs also contain
65 components of the homologous recombination machinery [13, 14] and associate with chromosome
66 ends [15] implicating these factors and structures in the underlying mechanisms of ALT. Indeed,
67 specifically-tagged telomeres were shown to be copied onto different chromosome ends in ALT cells
68 [16], supporting a role for recombination in ALT. Moreover, ALT can be suppressed by the abrogation
69 of the key recombination complex, Mre11:Rad50:Nbs1 (MRN) [17]. Finally, certain characteristics of
70 the ALT phenotype are consistent with recombination-mediated mechanisms for telomere elongation
71 including Break Induced Replication (BIR), rolling circle amplification and unequal sister chromatid
72 exchange [18, 19].

More recent work has uncovered a strong correlation between malignancies exhibiting the ALT phenotype and mutations in the Alpha Thalassemia/Mental Retardation Syndrome X-Linked (ATRX) gene [20, 21]. ATRX is a chaperone for histone H3.3, and along with Death Domain Associated Protein (DAXX), is responsible for H3.3's replication-independent incorporation into the genome [22, 23]. Specifically, H3.3 deposition into telomeric regions seems to be altered in ALT cells and, correspondingly, telomeric chromatin dynamics are altered [23-26]. How ATRX might contribute to the onset of ALT and why ALT appears to occur primarily in cells of mesenchymal origin is unclear [27]. The loss of ATRX, however, co-segregates with the ALT phenotype in cell fusion experiments [28]. Additionally, the frequency of ALT immortalisation events increases with the shRNA knock-down of ATRX in human fibroblasts [29, 30]. Lastly, ectopic re-expression of ATRX in ALT cells diminishes their ALT activity [30, 31].

In order to gain further insights into the mechanism of ALT, we have examined the earliest stages of telomeric elongation in the absence of ATRX during a telomere crisis in primary human fibroblasts and epithelial cancer cells. The absence of ATRX enabled the successful escape from crisis in fibroblasts, of mesenchymal origin, by the initiation of the ALT mechanism, whilst it compromised the ability of non-mesenchymal epithelial cells to escape crisis. However, epithelial cells in crisis exhibited manifestations of the ALT phenotype including the presence of C-circles, which were observed irrespective of whether they were capable of escaping crisis. Intriguingly, a sub-set of cells displayed specific telomeric elongation events, whereby the shortest telomeric alleles were subjected to elongation to chromosome-specific telomere lengths. Despite the presence of C-circles, this "ALT-like" telomeric elongation was not maintained, with elongated alleles ultimately being subjected to end-replication losses. Thus, the loss of ATRX combined with telomere dysfunction during crisis induces an ALT pathway, which confers replicative immortality in fibroblasts, but is transient in HCT116 epithelial cells. We also show an increase in non-canonical variant repeats in ALT telomeres compared to non-ALT controls.

99 **MATERIALS AND METHODS**

100 **Cell culture**

101 HCA2^{HPVE6E7} skin fibroblasts were provided by James Smith, Houston, US. They were cultured in DMEM
102 supplemented with 10% FCS, 2 mM glutamine, 0.1 mg/ml streptomycin, 100 U/ml penicillin and 4
103 µg/ml G418. Cells were cultured in T75 flasks and passaged every 7 days.

104 MRC5^{HPVE6E7} lung fibroblasts were obtained from the Coriell Institute cell repository [32]. They
105 were cultured in MEM supplemented with 10% FCS, 2 mM glutamine, 0.1 mg/ml streptomycin, 100
106 U/ml penicillin, 4 µg/ml G418, 1x NEAA, 3 mM NaOH and 0.2% $NaHCO_3$. Cells were cultured in T75
107 flasks and passaged every 7 days.

108 HCT116$^{ATRX-/0}$ cells [30] were cultured in McCoy's 5A medium supplemented with 10% FCS, 2 mM
109 glutamine, 0.1 mg/ml streptomycin, 100 U/ml penicillin and 4 µg/ml G418. Cells were cultured in T25
110 flasks and passaged every 7 days.

111 At each passage, samples were collected for cell counts to track population doublings (PDs), and
112 for DNA and protein extractions.

113

114 **CRISPR/Cas9 gene editing**

115 The ATRX gene was targeted by CRISPR/Cas9 gene editing in HCA2^{HPVE6E7} and MRC5^{HPVE6E7} cells [30].
116 The ATRX target sequence, 5'-GTTTCTGTCGGTCGCCTCAA-3', was used as the guide RNA to target exon
117 9 of the *ATRX* gene and ligated into a pSpCas9(BB)-2A-GFP plasmid (Addgene #48138) using Bbs1
118 restriction enzyme cut sites. 24 hr after nucleofection, cells were sorted according to GFP intensity by
119 flow cytometry and plated for single-cell cloning.

120

121 **Lentiviral transfection**

122 Retroviral transfections were used to transfect HCT116$^{ATRX-/0}$ cells with a dominant negative-hTERT
123 (DN-hTERT) cassette to abrogate telomerase activity. Recombinant retroviruses containing a pBABE-

124 puro vector (Addgene) encoding a DN-hTERT and puromycin selection genes were grown using ΨCRIP
125 cells, gifted by Richard Mulligan (Whitehead Institute, Cambridge) [33]. Cells that had successfully
126 integrated the vector were selected in puromycin 72 hr after addition of the retrovirus to the cells (2.5
127 µg/ml; Calbiochem) and medium containing puromycin was subsequently used for the culturing of
128 these cells. Expanded cells were ultimately plated for single-cell cloning.

129

130 **DNA extraction**

131 DNA was extracted using standard RNase A, Proteinase K and phenol:chloroform methods, [34]
132 ethanol precipitated, washed in 70% ethanol, air-dried, resuspended in 50 µl of 10 mM Tris-HCl and
133 quantified in triplicate using Hoechst fluorometry (Bio-Rad). A working stock of 20 µl at a
134 concentration of 10 ng/µl was made for each sample.

135

136 **STELA**

137 Single telomere length analysis (STELA) was undertaken as described [35]. Two primers were used to
138 amplify specific telomeres in the HCA2 model: XpYpE2 and 17p6. Three primers were used to amplify
139 specific telomeres in the MRC5 model: XpYpE2, XpYpAT and XpYpGC. Six primers were used to amplify
140 specific telomeres in the HCT116 model: XpYpC, 5p5, 7qK1, 8q2, 9p2 and 17pseq1rev. The PCR
141 conditions were as follows: 94°C for 20 s; 59°C (5p5, 17pseq1rev and 17p6), 61°C (9p2), 65°C (7qK1,
142 8q2, XpYpC, XpYpE2, XpYpAT and XpYpGC) for 30 s; 68°C for 8 min for 22 cycles. DNA fragments were
143 resolved with 0.5% TAE agarose gel electrophoresis and detected by Southern hybridisation at 55°C
144 overnight with a ^{32}P radiolabelled telomere repeat $(TTAGGG)_n$-containing probe together with probes
145 to detect the 1 kb and 2.5 kb markers. The blots were washed four times at 55°C with 0.1% SDS and
146 0.1X SSC, dried, exposed to a phosphor screen and scanned with a Typhoon FLA 9500 phosphoimager
147 (GE Healthcare) and analysed using ImageQuant TL (GE Healthcare).

148

149 **Fusion PCR**

150 Fusion PCR was undertaken as described [36]. Three primers were used to amplify inter- and intra-
151 allelic fusion events in the HCA2 model: 17p6, 21q1 and XpYpM. The PCR conditions were as follows:
152 94 °C for 20 s; 62 °C for 30 s; and 68 °C for 8 min and repeated for 25 cycles. DNA fragments were
153 resolved with 0.5% TAE agarose gel electrophoresis and detected by Southern hybridisation at 55°C
154 overnight with a ^{32}P radiolabelled chromosome-specific (17p, 21q and XpYp) probe together with
155 probes to detect the 1 kb and 2.5 kb markers. The blots were then washed four times at 55°C with
156 0.1% SDS and 0.1X SSC, dried, exposed to a phosphor screen and scanned with a Typhoon FLA 9500
157 phosphoimager (GE Healthcare) and analysed using ImageQuant TL (GE Healthcare).

158

159 **C-circle assay**

160 For detecting C-circles, 20 ng of genomic DNA was incubated with 7.5 U of ϕ29 DNA polymerase, 1
161 mM dATP, dGTP and dTTP, 0.2 mg/mL BSA, 0.1% Tween 20 and 1X ϕ29 buffer for 8 hr at 30°C as
162 described [37]. The samples were then denatured and slot blotted onto a positively-charged
163 hybridisation membrane (Hybond XL; GE Healthcare). The membranes were pre-hybridised in
164 Church's buffer (1% (w/v) BSA; 1 mM EDTA; 0.5 M phosphate buffer and 7% (w/v) SDS) and hybridised
165 overnight at 55°C with a ^{32}P radiolabelled telomere repeat $(TTAGGG)_n$ probe. The membranes were
166 then washed, dried, exposed, scanned and quantitated as described above.

167

168 **TRAP assay**

169 Telomerase activity in the HCT116 cell line was quantified using the TRAPeze XL telomerase detection
170 kit according to the manufacturer's instructions (Millipore). Protein was extracted using CHAPS lysis
171 buffer. Protein concentrations were determined by spectrophotometry and a working stock of 30 µl
172 at 100 ng/µl was prepared for each sample to be amplified by PCR. The excitation and emission state
173 wavelengths for fluorescein (485 nm and 535 nm, respectively) and sulforhodamine (585 nm and 620

174 nm, respectively) were measured on a Cytation3 plate reader (BioTek). All subsequent calculations
175 were done in GraphPad Prism 5 and telomerase activity was expressed as Total Product Generated
176 (TPG).

177 Telomerase activity in the HCA2 and MRC5 cell lines was quantified as described [38]. Following
178 protein extraction and quantification as described above, 500 ng of protein was incubated with 1X
179 TRAP buffer (2X stock: 40 mM Tris HCl pH 8; 3 mM $MgCl_2$; 126 mM KCl; 0.01% Tween 20; 2 mM EGTA;
180 0.2 mg/ml BSA; 0.1 mM dNTPs); 0.36 µM TS primer; 1 µl primer mix (stock 0.10 µM ACX primer; 0.19
181 µM NT primer; and 0.0025 pM TSNT internal control primer: 5'-
182 AATCCGTCGAGCAGAGTTAAAAGGCCGAGAAGCGAT-3'); 0.4X Titanium Taq polymerase (Clontech); and
183 ddH_2O to make up 50 µl. Reactions were processed using a Tetrad thermal cycler (Bio-Rad) at the
184 following conditions: 25°C for 40 min; 95°C for 5 min for 1 cycle; 95°C for 30 s; 52°C for 30 s; and 72°C
185 for 45 s for 29 cycles followed by 72°C for 10 min for 1 cycle. 10 µl of 6X Ficoll gel loading solution (5%
186 bromophenol blue; 5% xylene; and 15% Ficoll) were added to each reaction. TRAP PCR products were
187 resolved on acrylamide gels (12.5% acrylamide 19:1; 0.06% APS; 0.125% TEMED; and 0.6X Tris-borate-
188 EDTA (TBE)). Gels were electrophoresed in 1X TBE (400 ml of dH_2O and 100 ml of 5X TBE stock: 0.45
189 M Tris; 0.45 M boric acid; and 10 mM EDTA pH 8) for 1 to 2 hrs at 100 V. To visualise telomerase
190 activity, gels were incubated in 1:10,000 SYBR-gold for 10 min on a rocker at room temperature. Gels
191 were then scanned using the typhoon FLA 9500 scanner using the SYBR-Gold filter (473 nm laser
192 wavelength; 200 micron pixel size).

193

194 **Oligonucleotides**

195 Telorette2; 5'-TGCTCCGTGCATCTGGCATCTAACCCT-3'
196 Teltail; 5'-TGCTCCGTGCATCTGGCAT-3'
197 5p5; 5'-GGAGCAGCATTCTCTTCACCACAG-3'
198 7qK1; 5'-GGGCACTGCCTCGCTTTGA-3'
199 9p2; 5'-CACATTCCTCATGTGCTTACG-3'

200 17pseq1rev; 5'-GAATCCACGGATTGCTTTGTGTAC-3'

201 17p6; 5'-GGCTGAACTATAGCCTCTGC-3'

202 21q1; 5'-CTTGGTGTCGAGAGAGGTAG-3'

203 XpYpC; 5'-CAGGGACCGGGACAAATAGAC-3'

204 XpYpE2; 5'-TTGTCTCAGGGTCCTAGTG-3'

205 XpYp-427G/415C; 5'-GGTTATCGACCAGGTGCTCC-3'

206 XpYp-427A/415T; 5'-GGTTATCAACCAGGTGCTCT-3'

207 XpYpM; 5'-ACCAGGTTTTCCAGTGTGTT-3'

208

209 **Whole genome sequencing**

210 27 HCT116 DNA samples (a combination of ALT-positive and telomerase-positive clones) were whole
211 genome sequenced using the BGISEQ-500 platform, providing paired end (2X 100 bps) sequencing
212 with a 15X coverage. A minimum of 20 µl at a concentration of 1 µg per sample was assayed. The QC,
213 library preparation, sequencing and data filtering were carried out by BGI. Sequence mapping and
214 analysis were carried out as described [39].

215

216 **PacBio SMRT sequencing analysis — generation of sequencing samples**

217 To generate PCR amplicons to be sequenced, specific chromosome ends were amplified using STELA.
218 A minimum of 500 ng of DNA were required for PacBio sequencing and therefore 1,600 reactions were
219 generated for each sample. To amplify multiple telomeres in one reaction, multiple primers were
220 added to the master mix (XpYpC, 7qK1 and 17pseq1rev for HCT116 samples; XpYpE2 and 17p6 for
221 HCA2 samples; and XpYpE2 and 17pseq1rev for the U2OS sample) adjusting the volume of ddH_2O
222 accordingly to limit the amount of input genomic DNA for optimal sequencing. The reactions were
223 processed using a Tetrad thermal cycler (Bio-Rad) at the following conditions: 94°C for 20 s; 63°C for
224 30 s; and 68°C for 8 min for 24 cycles. Following PCR amplification, sample reactions were pooled
225 together and concentrated using an ISS110 Speedvac system (Thermo Fisher Scientific) to evaporate
226 excess water using a vacuum. All samples were then purified using AMPure XP beads (Beckman

227 Coulter) according to the manufacturer's manual. Samples were then processed for PacBio library
228 preparations.

229

230 **PacBio SMRT sequencing analysis — data processing**

231 The raw reads were filtered to retain only reads with a sub-telomere primer at one end and a telorette
232 primer at the other end. This was accomplished by aligning the reads using Edlib. Then, all sequences
233 were labelled using a Hidden Markov Model (HMM) to highlight and dissociate telomere repeat
234 arrays, sub-telomere sequences and insertions. Sequences were broken down into 6 bp kmers and
235 given scores upon comparison to the canonical telomere repeat TTAGGG allowing an edit distance of
236 2 bps. The scores were as follows: 0 for background sequence (sub-telomere and insertions); 1 for
237 forward strand telomere repeats (CCCTAA); and 2 for reverse strand telomere repeats (TTAGGG).
238 Therefore, variant repeats with a maximum of 2 bp substitutions compared to TTAGGG were classed
239 as telomere sequence. To clean the data further, subsequent filtering steps were added to the
240 pipeline, which were aimed at removing sequencing and PCR artefacts generated during the process.
241 By this means, the following classes of reads were removed from the analysis: unexpected non-sub-
242 telomeric sequences amplified by low homology with primers; STELA products that appeared to have
243 undergone primer swapping; products that did not have a detectable sub-telomere sequence; and
244 concatemers of STELA products. All of the retained sequences were then compiled into an Excel
245 spreadsheet for manual curation and analysis. The spreadsheet included the sub-telomere length,
246 trimmed telomere length as well as the extension lengths and sequences amongst other features.
247 More detail of the methods used can be found in S1 Methods.

248

249 **RESULTS**

250 **The loss of ATRX induces crisis survival through ALT in primary human fibroblasts.**

251 We examined telomere dynamics during crisis in the absence of ATRX and queried whether this
252 impacts the ability of mesenchymal cells to achieve replicative immortality. Telomere crisis was
253 initiated in two primary fibroblast cell lines, HCA2 skin fibroblasts and MRC5 lung fibroblasts, following
254 infection with amphotropic retroviral vectors encoding HPV16 E6 and E7 to abrogate TP53 and
255 retinoblastoma (Rb). Approximately 20 to 30 population doublings (PDs) prior to the onset of crisis,
256 an ATRX-targeted Clustered Regularly Interspaced Palindromic Repeat/CRISPR-associated 9
257 (CRISPR/Cas9) vector was used to functionally inactivate the ATRX gene [30]. Following transfection
258 with the ATRX CRISPR/Cas9 vector, single-cell clones were isolated and monitored as they transited
259 through crisis (Figs 1A and 1B and S1A and S1B). A total of 6 and 9 clones survived crisis for the HCA2
260 and MRC5 cell lines respectively (11.5% and 7.1% survival rate, n=52 and n= 127 respectively). ATRX
261 protein expression was monitored by Western blot analysis to establish the effects of the CRISPR
262 vector on cell survival. Strikingly, clones that retained ATRX protein expression failed to escape crisis,
263 whilst a complete loss of the ATRX protein resulted in replicative immortality in both cell lines (Figs 1C
264 and 1D and S1C). The status of the ATRX gene was sequence verified in two randomly selected clones:
265 clone 10 and clone 18, which confirmed that a clone (clone 10) that did not escape, expressed wild-
266 type ATRX (likely due to incomplete cutting by CRISPR) whereas a clone that did escape (clone 18), did
267 not express ATRX due to a -2 bp frameshift (S2 Fig).

268 The immortalisation was dependent upon the loss of ATRX expression as, consistent with
269 numerous previous observations [35, 40], $HCA2^{HPVE6E7}$ control clones (n = 6), which express a WT ATRX
270 failed to escape crisis and died after a prolonged period of crisis (S3 Fig). In conclusion, it appeared as
271 if even low-level residual ATRX activity hindered the ability of cells to escape crisis whereas a complete
272 loss of ATRX correlated with successful long-term survival (*i.e.*, immortalisation) in primary human
273 fibroblasts (Figs 1A-D and S1A-C)).

274 Telomere dynamics were analysed at the XpYp and 17p chromosome ends using STELA (Figs 1E
275 and 1F and S1D and S1E; and S4). Consistent with previous observations in clonal WT fibroblast
276 cultures [35, 41], homogeneous allelic telomere-length distributions were observed in clones that
277 failed to escape crisis, as well as control clones, with all telomeric alleles exhibiting a gradual loss of
278 telomere length as cells approached crisis (Figs 1E and S1D and S4). In stark contrast, the clones that
279 escaped crisis upon loss of ATRX displayed heterogeneous telomere lengths, with no distinguishable
280 allelic telomere length distributions, even at the earliest sampling points (Figs 1F and S1E and S5).
281 MRC5 cells exhibit telomere-adjacent sequence polymorphisms that allow for allele-specific (GC or
282 AT) STELA at the XpYp telomere [41]. MRC5 clones 121, 9 and 46 that escaped crisis in the absence of
283 ATRX, displayed heterogeneous telomere-length distributions at both alleles (S1E and S5B Figs), in
284 contrast to clone 1, that failed to escape crisis and maintained distinct homogeneous allelic
285 distributions (S1D Figs). Therefore, the loss of ATRX induces telomere length heterogeneity during
286 crisis at both alleles, irrespective of their length prior to crisis, and this heterogeneity is maintained
287 following their escape from crisis, suggesting that these cells may have induced an ALT-like phenotype.

288 Telomere fusion analysis of HCA2 clones revealed that fusion events could readily be detected,
289 even at the earliest sampling points, indicating that these cells had entered a telomere crisis and thus
290 the generation of telomere length heterogeneity occurs within the period of crisis (S6 Fig). These data
291 also demonstrate that short telomeres during crisis, in the absence of ATRX, are subjected to repair
292 activity, as observed in wild-type cells undergoing crisis [33, 35]. Moreover, as the cells escaped crisis,
293 the frequency of fusion events was reduced in all but one clone (S6B Fig; clone 49) and the analysis of
294 post-crisis ALT^+ U2OS cells revealed no detectable telomere fusion events despite these cells
295 exhibiting extreme telomere length heterogeneity. These data indicate that the telomere fusions
296 occur early in crisis and that this is likely necessary (clones 18, 21, 27, 28 and 49) but not sufficient
297 (clone 1) for the establishment of an ALT phenotype. Moreover, the data indicate that once ALT is
298 established, it is sufficient to prevent the subsequent fusion of short telomeres even though they are
299 relatively abundant.

300 One of the hallmarks of ALT is the presence of extrachromosomal partially single-stranded DNA,
301 referred to as C-circles [37]. We used a C-circle assay to establish whether the telomere elongation
302 events observed during crisis may coincide with the presence of C-circles and thus be consistent with
303 ALT activity [37]. C-circles were absent in the parental HCA2 and MRC5 cells, but increased during the
304 escape from crisis in all HCA2$^{HPVE6E7;ATRX-/o}$ and MRC5$^{HPVE6E7;ATRX-/o}$ clones to levels greater than that
305 observed in the ALT-positive control U2OS (Figs 1G, S1F and S7). In contrast, clones that failed to
306 escape crisis were negative for C-circles. In addition, telomerase activity was not detected in any of
307 the fibroblast clones following immortalisation, irrespective of whether they subsequently escaped
308 crisis or not (S8 Fig). Taken together these data reveal a key role for ATRX in suppressing the ability of
309 fibroblast cells to escape a telomere-driven crisis by normally inhibiting telomeric elongation events
310 during crisis. Moreover, the induction of ALT activity is sufficient to ultimately confer functional
311 telomeres that, subsequent to crisis survival, are no longer subjected to fusion.

312

313 **ATRX facilitates the escape from a telomere-driven crisis in epithelial cancer cells.**

314 We have previously generated ATRX-null telomerase-positive human HCT116 colorectal epithelial
315 cancer cells using both recombinant adeno-associated virus (rAAV)- and CRISPR/Cas9-mediated gene
316 targeting [30]. We demonstrated that the genetic deletion of ATRX alone did not lead to the activation
317 of the ALT phenotype even when these cells were forced through crisis; these cells were negative for
318 C-circles, did not display heterogenous telomere length profiles and continued to express telomerase
319 [30]. Thus, the loss of ATRX had a different outcome for the non-mesenchymal HCT116 epithelial cells
320 than it did for the mesenchymal HCA2 and MRC5 fibroblast cell lines. To assess whether the loss of
321 ATRX combined with telomere dysfunction during crisis could at least initiate the ALT mechanism for
322 survival we transfected HCT116$^{ATRX-/o}$ with a dominant-negative hTERT (DN-hTERT) construct [42] to
323 abrogate telomerase activity and induce a telomere-driven crisis. A total of 149 single cell clones were
324 picked from four separate DN-hTERT transfections; clones were continuously passaged in culture and
325 were monitored for changes in growth rate and morphology. All the clones entered a period of crisis,

326 defined as a slowing in the rate of expansion of the culture (Fig 2A) and a change in morphology from
327 small, actively-dividing cells to large, multi-nucleated cells (S9 Fig). Unlike WT HCT116$^{DN\text{-}hTERT}$ clones,
328 in which 100% of clones (11 of 11) rapidly escaped crisis after having re-established telomerase activity
329 [33], only 33 out of 149 (22%) of the HCT116$^{ATRX\text{-}/o:DN\text{-}hTERT}$ clones escaped a telomere-driven crisis and
330 appeared to gain replicative immortality (Fig 2A). These 33 clones, of which 29 appeared to be
331 telomerase positive and 4 ALT, were cultured until a normal growth rate had resumed after which the
332 cultures were terminated. The remaining 116 clones entered crisis and died, including 38 clones that
333 entered crisis prior to a sample being taken (summarised in S1 Table). No evidence of crisis was
334 observed in HCT116$^{ATRX\text{-}/o:Puro}$ control clones (n = 12) expressing the puromycin drug resistance
335 selection cassette (*i.e.*, without DN-hTERT) only (S10 Fig). Thus, the absence of ATRX compromised the
336 ability of HCT116 epithelial cells to escape crisis (where only 22% of the ATRX-null clones escaped
337 crisis) — a phenotype diametrically opposed to the one observed in fibroblast cells, where 100% of
338 the surviving clones were ATRX-null.

339

340 **Specific telomeric elongation events and C-circles consistent with ALT activity in the absence of**
341 **ATRX.**

342 We monitored the telomere dynamics of HCT116$^{ATRX\text{-}/0:DN\text{-}hTERT}$ clones undergoing crisis in culture.
343 Telomere length profiles at the 17p and XpYp chromosome ends were obtained using STELA at
344 sampling points both pre- and post-crisis for 82 clones. The majority of clones (78 clones: 95%)
345 exhibited telomere erosion prior to crisis (mean of 60 bps/PD at 17p and 80 bps/PD at XpYp),
346 consistent with the abrogation of telomerase activity following the expression of DN-hTERT. Strikingly,
347 three clones displayed telomere erosion followed by, at the point of crisis, an abrupt elongation event
348 at both chromosome ends analysed (mean of elongated allele: 6.68 kb at 17p and 1.87 kb at XpYp)
349 (Fig 2B and 2C, clones 2, 3 and 4). A fourth clone exhibited a similar sized elongation event at the XpYp
350 chromosome end (1.07 kb), but not at 17p (S11 Fig). The bimodal distributions observed at the 17p
351 chromosome end before crisis were consistent with allelic telomere length variation, we thus

352 considered that the elongated telomeres arose from the extension of a single allele. However, it was
353 also possible that the bimodal distributions arose from subsets of cells with distinct telomere length
354 profiles with the extension events occurring in a specific subset of cells and were thus not allelic. To
355 test this, we subcloned clone 3 at the point of crisis and examined the telomere length distributions.
356 All the surviving subclones displayed bi-modal telomere length distributions, consistent with allele-
357 specific telomeric elongation (S12 Fig). Interestingly, a single subclone died (subclone 2) at PD17 whilst
358 displaying no telomere extension events (S12 Fig).

359 The clones that failed to escape crisis, showed telomere erosion prior to crisis, but no change in
360 telomere length at crisis (Figs 2B and 2C, clones 1 and 8 and S13). HCT116$^{ATRX-/o:Puro}$ control clones
361 displayed no significant change in mean telomere length (Fig 2B and 2C). A further 17 clones that
362 escaped crisis, exhibited a change from homogeneous to more heterogeneous telomere-length
363 distributions, whilst clones for which no sample was available pre-crisis (n = 8) also showed similar
364 heterogeneity post-crisis (S14 Fig), these telomere dynamics are consistent with a reactivation of
365 telomerase following the escape from crisis, as described [33].

366 We next examined the longer-term maintenance of the extended telomeres in the three
367 clones that had exhibited elongation at both chromosome ends studied. These clones were kept in
368 culture for 219 days until they had obtained over 100 PDs and the telomere length profiles were
369 examined at serial sampling points. At the 17p telomere, we observed bi-modal telomere-length
370 distributions pre- and post-crisis consistent with two telomeric alleles [41]. We hypothesised that the
371 short allele, prior to crisis, became elongated to a mean of 6.68 kb (*i.e.*, an extension of 5.40 kb) whilst
372 the longer allele continued to erode (Fig 3A). At the XpYp telomere, a single allele was detected that
373 underwent elongation to a mean of 1.87 kb (*i.e.,* an extension of 1.06 kb) (S15 Fig). Following the initial
374 elongation event, both telomeres continued to erode, with the longer telomeric allele at 17p
375 exhibiting an erosion rate (mean for all 3 clones examined: 83 bps/PD, Fig 3A) that was
376 indistinguishable from that observed in primary cells in the absence of telomerase [41], whilst the
377 shorter 17p telomeric alleles exhibited a slower rate of erosion (mean for all 3 clones examined: 29

378 bps/PD). The single XpYp telomeric allele was also subject to telomere erosion (mean rate of erosion
379 of 27 bps/PD; S15 Fig). Telomere erosion continued until the cultures upregulated telomerase at PD
380 59, 60 and 58 in clones 2, 3 and 4, respectively, as determined by the TRAP assay. The restoration of
381 telomerase activity was accompanied by an increase in the heterogeneity of the telomere length
382 distributions resulting in a loss of bimodal distributions and an increase in mean telomere length (Fig
383 3A and 3B). These telomere dynamics were recapitulated in subclone 11 and were consistent with the
384 action of telomerase preferentially elongating the shorter allele, but not the longer allele (S12 Fig) [36,
385 43].

386 To assess if the initial elongation event observed was consistent with ALT upregulation, clones
387 were subjected to the C-circle assay. The intensity of the signal was quantified in duplicate and all
388 results were normalised to the HCT116$^{ATRX-/o}$ parental cell line background. The three clones (clones 2,
389 3 and 4) that displayed elongation at the XpYp and 17p telomeres showed a gradual increase in C-
390 circles from the initial telomere elongation event, although these cells continued to exhibit C-circles
391 during the re-establishment of telomerase activity (Fig 3C). A further 3 clones (32, 48 and 131), for
392 which no telomeric elongation event was observed at the XpYp telomeres, were also strongly positive
393 for C-circles post-crisis, a state which diminished at later PDs (S16A-C Fig); these cells also upregulated
394 telomerase activity (S16D Fig). Overall the levels of C-circles was consistently less than that observed
395 in the ALT-positive cell line U2OS and less than that observed in fibroblast cultures (S7 Fig). In
396 summary, the presence of C-circles correlated with the ALT-like telomere elongations observed in
397 clones 2, 3 and 4 but C-circles were also present in clones 32, 48 and 131, which did not elongate.
398 Thus, we concluded that while the presence of C-circles might be necessary for these ALT-like
399 elongations, they aren't sufficient.

400 It was clear that in the HCT116$^{ATRX-/o:DN-hTERT}$ system, single telomeric elongation events were not
401 sufficient to confer replicative immortality following the escape from crisis. We therefore considered
402 that other clones that failed to escape crisis may also have shown evidence of telomeric elongation
403 events. On this basis, STELA profiles were obtained at 17p and XpYp for all clones that died and for

404 which samples where available (n = 46). Two clones (108 and 132) exhibited elongation events at the
405 XpYp telomere of 0.74 kb on average, similar to that observed in clones 2, 3, 4 and 147 (S17A Fig). No
406 evidence of telomeric extension was observed at the 17p chromosome end in these two clones,
407 instead the shorter telomeric allele was lost during crisis (S17B Fig). Both these clones were positive
408 for C-circles (S17C and F17D Fig) whilst telomerase activity was undetectable (S17D Fig). Importantly,
409 these data imply that neither C-circle activity, nor single telomeric elongation, is sufficient for these
410 cells to escape a telomere-driven crisis. All HCT116$^{ATRX-/o:DN-hTERT}$ clones that ultimately obtained
411 replicative immortality did so by regaining telomerase as their principle TMM.

412 Overall, these data indicate that the combination of the loss of ATRX and telomere dysfunction
413 during crisis is sufficient to initiate an "ALT-like" mechanism in a subset of clones (21% of surviving
414 clones and 16% of clones that died; 19% of total clones). Whilst this rapid telomere elongation and C-
415 circle activity is "ALT-like", in the HCT116 DN-hTERT model system this is insufficient for the
416 maintenance of ALT activity and telomerase activity is ultimately required for long-term survival.

417

418 **Chromosome specific elongation.**

419 Having observed telomeric elongation events in multiple HCT116$^{ATRX-/o:DN-hTERT}$ clones that appeared to
420 be chromosome specific, with a mean of 5.40 kb added to the shorter allele at 17p and 1.06 kb at the
421 single XpYp allele (Fig 2B and 2C), we investigated whether chromosome-specific telomeric elongation
422 events occurred at other chromosome ends. To address this, we applied STELA at the 5p, 7q, 8q and
423 9p chromosome ends in clones that showed telomere elongation at both the XpYp and 17p
424 chromosome ends (clones 2, 3 and 4) (Figs 4 and S18). We observed specific elongation events in all
425 three clones at the 5p, 7q and 9p telomeres, with mean extensions to: 3.58 kb (extension of 1.9 kb) at
426 5p; 3.22 kb (extension of 1.14 kb) at 7q; 1.93 kb (extension of 0.52 kb) at 9p (S18D Fig). In contrast, no
427 extension events were observed at the telomeres at the 8q chromosome end, which were long relative
428 to the other telomeres analysed (6.66 kb) in the parental cell line; instead, this telomere simply eroded
429 as a function of cell division post-crisis. Thus, there appeared to be a lack of unified specificity in the

430 telomere elongation, with 5 of the 6 telomere ends examined demonstrating telomere elongation.
431 With that said, there clearly was a rather profound difference in the amount of telomere elongation
432 associated with each end, ranging from a ~5.5 kb addition at 17p to only ~0.5 kb at 9p. The basis for
433 the variable elongation is not understood, but most chromosome ends appeared affected.

434

435 **Elongation affects all alleles and arises from multiple independent events.**

436 Our STELA data indicated that some HCT116 clones might be ALT-like and that short telomeric alleles
437 were specifically elongated during crisis. To establish if this was the case, and to examine the nature
438 of telomere-specific extensions, we characterised telomeric alleles using PacBio single-molecule real
439 time (SMRT) long-read sequencing of multiplexed STELA amplicons from the 7q, 17p and XpYp
440 telomeres obtained by pooling 1,600 reactions for each sample analysed (HCT116$^{ATRX-/o}$ parental and
441 clone 3; HCA2^{HPVE6E7} parental and clone 21$^{ATRX-/o}$; and U2OS). We utilised the hypervariable telomere
442 variant repeat (TVR) patterns within the first 100 base pairs of the telomere repeat array to
443 differentiate telomeric alleles from HCT116, HCA2 and U2OS cells [44-46]. The TVR content was
444 determined for each read to establish any differences in variant repeat distributions between the ALT-
445 like clones and their respective parental controls. We observed an overall increase in TVRs in the ALT-
446 like clone, with a specific enrichment of TTCGGG TVR in the HCT116 clone at all chromosome ends
447 and alleles analysed (S19A Fig), whilst an increase in the TGAGGG TVR was observed in the HCA2 clone
448 analysed that was most apparent at the XpYp chromosome end (S19B Fig). Consistent with previous
449 findings [47], the telomeric alleles in U2OS contained relatively few TVRs being composed
450 predominately of TTAGGG repeats (S19C Fig). These data indicated that the increase in TVR
451 interspersion patterns were specific to each cell clone and consistent with a utilisation of a clone-
452 specific telomeric DNA template.

453 Examination of the sequence composition of individual telomeric alleles revealed several notable
454 features (Figs 5 and S20). In HCT116 cells, a dramatic increase in TTCGGG variant repeats was observed
455 in all alleles, at each of the three telomeres analysed, irrespective of the length of the elongated allele.

456 In HCA2 cells, an insertion of a characteristic TGAGGG interspersion pattern was observed in XpYp
457 allele 1, with different TVR patterns in XpYp allele 2 and both 17p alleles sequenced. Together these
458 observations indicate that the insertion of TVRs does not lead to specific elongation events, with
459 alleles exhibiting changes in TVR composition in the absence of elongation events. Moreover, each
460 individual telomere sequenced displayed distinct TVR interspersion patterns that disrupted the
461 parental allele at different points with respect to the beginning of the telomere repeat array. These
462 data indicate the occurrence of multiple different mutational events, occurring within different
463 telomeric alleles, with the majority of events resulting in the replacement of distal sequences, leaving
464 the repeat distributions at the beginning of the telomere repeat array intact (Figs 5 and S20). The
465 diversity of TVR distributions within a cell and between cells that escape crisis in the absence of ATRX
466 is consistent with the view that telomeric mutation during crisis occurs multiple times and in multiple
467 independent cells.

468

469 **Initiation of ALT in HCT116$^{ATRX-/o:DNhTERT}$ is not associated with increased genomic complexity.**

470 The transit through a telomere crisis is associated with the induction of increased genomic complexity
471 with distinct topologies observed in the context of specific DNA repair deficiencies [33, 39, 48]. We
472 therefore examined whether the absence of ATRX modulates genomic complexity in cells that escape
473 crisis and whether this was impacted by the telomeric elongation events observed. We generated
474 whole genome sequence data from HCT116$^{ATRX-/o:DNhTERT}$ clones that exhibited "ALT-like" telomere
475 elongation, sampling the cells pre- and post-crisis. We also analysed clones that showed no evidence
476 of telomere elongation, nor C-circles, but had upregulated telomerase activity during crisis (total n =
477 30). All HCT116$^{ATRX-/o:DNhTERT}$ clones displayed genome stability prior to crisis, as did all the clones that
478 exhibited transient "ALT-like" activity. Consistent with our previous observations [39], all the
479 HCT116$^{ATRX-/o:DNhTERT}$ clones that had upregulated telomerase showed a higher rate of structural
480 variants, including an example of chromothripsis (S21 Fig). Thus, whilst the initiation of "ALT-like"
481 activity in HCT116$^{ATRX-/o:DNhTERT}$ cells undergoing crisis in the absence of ATRX is associated with rapid,

482 telomere-specific elongation, this did not appear to be accompanied by large-scale genomic copy
483 number changes, or at least no more so than was observed in immortalised clones lacking the “ALT-
484 like” phenotype.

485

486 **DISCUSSION**

487

488 A strong link between ATRX and the ALT phenotype in various malignancies and cell culture models
489 has been well established [21, 28, 30, 49]. Whilst there has been a focus on the association of ATRX
490 with such phenotypes or mechanistic contributions to repressing ALT activity, thus far it has only been
491 demonstrated once that the loss ATRX alone is sufficient to induce ALT, and only in specific glioma cell
492 lines [50]. This lack of ALT inducing-activity in ATRX-null cells was surprising particularly given the
493 association of the lack of ATRX expression with ALT cancers. Adding to this complexity was the finding
494 that genetic ablation of another histone H3.3-H4 dimer chaperone, anti-silencing function 1 (ASF-1),
495 readily generated ALT-activity in telomerase-positive cells [51]. Here we show that the loss of ATRX
496 allows primary human fibroblast cultures undergoing a telomere-driven crisis to readily escape and
497 gain replicative immortality, following the establishment of ALT-activity. Importantly, even low-level,
498 residual ATRX activity, is sufficient to prevent these cells from initiating ALT and achieving immortality
499 (Fig 2C). In contrast, the loss of ATRX alone was not sufficient to induce ALT in epithelial cancer cells
500 when experimentally manipulated to undergo a second crisis. Nonetheless, even in these cells, an
501 "ALT-like" phenotype could be initiated, albeit ultimately not stably maintained. These data are
502 consistent with the view, that ATRX is a *bona fide* ALT inhibitor in the context of telomere dysfunction
503 [31]. Moreover, by demonstrating that there are different immortalisation outcomes depending upon
504 the type of cell in which the loss of ATRX activity occurs, we provide clarity to a literature that was
505 opaque.

506 ATRX plays an important role in replication fork protection and restart, and its loss leads to an
507 increase in replication fork stalling and collapse [52, 53]. Furthermore, ATRX, along with its binding
508 partner DAXX, prevents the accumulation of secondary structures such as R-loops and G quadruplexes,
509 that arise at repetitive regions of the genome (including telomeres), by incorporating histone H3.3
510 into nucleosomes [54, 55]. These secondary structures form a further barrier to the replication fork
511 machinery thereby increasing replication stress, which can be repaired by BIR [54, 56]. Somewhat
512 counterintuitively, replication stress is actually required in ALT cells because the repair induced by BIR

513 leads to telomeric elongation. We therefore propose that the loss of ATRX and the presence of short
514 telomeres during crisis may trigger telomere lengthening via the accumulation of replication stress
515 and the induction of BIR at telomeres [57]. A corollary of this conclusion is that the factors required
516 for replication stress and/or BIR are likely to vary between fibroblasts (more permissive) and epithelial
517 (non-permissive) cells. Our model also postulates that mutations that diminish or inactivate BIR are
518 likely to impede the establishment of ALT; a model that we are currently trying to test. While we
519 believe that differences in BIR is the most likely, and parsimonious, explanation for the cell type and
520 TMM disparities observed in these studies, it should be emphasised that the distinction between
521 fibroblastic and epithelial cell lines we have observed could also be related to the fact that the HCA2
522 and MRC5 fibroblast cell lines had not, unlike the HCT116 epithelial cell line, undergone a previous
523 transformation event. The impact of a previous transformation event on the ability of a cell to
524 establish a new TMM is unknown, but clearly worth future investigation.

525 Our data show that the ALT mechanism induces elongation events at multiple chromosome ends
526 only in cells that have entered a telomere-driven crisis. In fibroblasts, telomere lengthening and
527 heterogeneity were observed in all telomeric alleles, whereas in epithelial cancer cells, lengthening
528 appeared to be more specific to the shortest alleles. The underlying mechanism for these differences
529 is not apparent from our data, although, it has recently been shown, through single molecule analysis,
530 that telomere length and content heterogeneity varied according to the sub-telomere studied in a
531 panel of ALT cell lines [58], consistent with chromosome-specific events. However, our study suggests
532 a different possibility; namely that the difference may be a manifestation of different levels of BIR
533 factors/ALT activity given that fibroblasts fully activated the ALT pathway, whereas, the cancer
534 epithelial cells only transiently activated it. In this situation, the extreme telomere length
535 heterogeneity generated following the full activation of the ALT pathway may mask subtler and
536 specific elongation events that may be more apparent at lower levels of activity. Interestingly, our
537 data suggest that these events are chromosome specific, as independent clones exhibited similar
538 elongation events at each telomere in the HCT116 model. We hypothesise that telomeric elongation
539 may be regulated, with a specific and consistent DNA fragment length, consisting of telomere variant

540 repeats derived from telomeric and interstitial telomeric sequences [59] being inserted into the
541 telomere, potentially mediated by a recombination-based mechanism [16, 19, 60-62] and/or by BIR,
542 which is known to be highly mutagenic. Consistent with recombination-based mechanisms, a recent
543 study has shown the presence of large linear extrachromosomal DNA, alongside the C-circles and short
544 linear tracts already well established as ALT markers, that accounts for 40% of the total telomere signal
545 in U2OS. These DNA structures have the potential to play an active role in telomere maintenance by
546 acting as templates in BIR-mediated lengthening [58].

547 Alterations in TVR patterns in ALT clones were specific to each cell clone,, which is consistent with
548 previous studies investigating the telomere repeat content in ALT-positive cancer samples [63, 64].
549 We therefore hypothesise that a common initiating event is required to seed the clone-specific TVR
550 patterns, forming ALT precursors as described in yeast models [62] that subsequently provide a
551 template to enable elongation of short telomeres by inter-allelic exchanges [16, 61]. Interestingly, TVR
552 replacement was also observed both proximally and distally to distinctive conserved TVR patterns
553 (highlighted in red, Fig 5), indicating a possible gene conversion type mechanism that can conserve
554 existing TVR patterns, although this remains to be fully tested. Whilst normal human cells harbour
555 non-canonical variant repeat interspersion patterns within the proximal 2 kb of the telomere repeat
556 array [45], ALT telomeres display TVRs throughout the telomere [65]. It is considered that these enable
557 the anchoring of nuclear receptors such as COUP-TF2, which play a role in the ALT phenotype [65].
558 We observed a similar interspersion pattern of variant repeats in the fibroblast ALT-like clones.
559 Interestingly, PacBio sequencing of the HCT116 ALT-like clones showed a stark increase in the TTCGGG
560 variant repeat, even at the distal end of the chromosome. The presence of these non-canonical TVRs
561 may reduce the binding of the telomere-associated proteins telomere recognition factors 1 and 2
562 (TRF1 and TRF2) to the telomere and compromise telomere function. Despite that our data provides
563 some insight in telomere variant repeat pattern content, more remains to be done to elucidate the
564 mechanism of elongation in the context of ALT.

565 In summary, in fibroblasts, the induction of ALT in the absence of ATRX occurs early in crisis at
566 the point that telomere fusions are detected. This facilitates a rapid and efficient escape from crisis,
567 the abrogation of telomere fusions and genomic stabilisation. We suggest these may represent the
568 types of events that occur during the initiation of ALT-positive tumours. Further understanding of the
569 upregulation of the ALT pathway and the mechanism of elongation is crucial for the development of
570 treatments as well as diagnostic and prognostic tests.

571 **Acknowledgements**

572 We thank Joanne Morgan, MRC Centre for Neuropsychiatric Genetics and Genomics, Cardiff University
573 for PacBio sequence analysis. We thank members of the Baird and Hendrickson laboratories for help
574 and advice.

575

576 **REFERENCES**

577 1. O'Sullivan RJ, Karlseder J. Telomeres: protecting chromosomes against genome instability.
578 Nat Rev Mol Cell Biol. 2010;11(3):171-81. Epub 2010/02/04. doi: 10.1038/nrm2848

579 10.1038/nrm2848. Epub 2010 Feb 3. PubMed PMID: 20125188; PubMed Central PMCID:
580 PMCPMC2842081.
581 2. Olovnikov AM. A theory of marginotomy. The incomplete copying of template margin in
582 enzymic synthesis of polynucleotides and biological significance of the phenomenon. J Theor Biol.
583 1973;41(1):181-90. Epub 1973/09/14. PubMed PMID: 4754905.
584 3. Wright WE, Shay JW. The two-stage mechanism controlling cellular senescence and
585 immortalization. Exp Gerontol. 1992;27(4):383-9. Epub 1992/07/01. PubMed PMID: 1333985.
586 4. Lin TT, Letsolo BT, Jones RE, Rowson J, Pratt G, Hewamana S, et al. Telomere dysfunction
587 and fusion during the progression of chronic lymphocytic leukemia: evidence for a telomere crisis.
588 Blood. 2010;116(11):1899-907. doi: 10.1182/blood-2010-02-272104. PubMed PMID: 20538793.
589 5. Roger L, Jones RE, Heppel NH, Williams GT, Sampson JR, Baird DM. Extensive telomere
590 erosion in the initiation of colorectal adenomas and its association with chromosomal instability. J
591 Natl Cancer Inst. 2013;105(16):1202-11. Epub 2013/08/07. doi: 10.1093/jnci/djt191. PubMed PMID:
592 23918447.
593 6. Ju Z, Lenhard Rudolph K. Telomere dysfunction and stem cell ageing. Biochimie.
594 2008;90(1):24-32. doi: 10.1016/j.biochi.2007.09.006. PubMed PMID: 18029082.
595 7. Hanahan D, Weinberg RA. The hallmarks of cancer. Cell. 2000;100(1):57-70. PubMed PMID:
596 10647931.
597 8. Henson JD, Reddel RR. Assaying and investigating Alternative Lengthening of Telomeres
598 activity in human cells and cancers. FEBS Lett. 2010;584(17):3800-11. Epub 2010/06/15. doi:
599 10.1016/j.febslet.2010.06.009

600 10.1016/j.febslet.2010.06.009. Epub 2010 Jun 11. PubMed PMID: 20542034.
601 9. Shay JW, Reddel RR, Wright WE. Cancer. Cancer and telomeres--an ALTernative to
602 telomerase. Science. 2012;336(6087):1388-90. doi: 10.1126/science.1222394. PubMed PMID:
603 22700908.
604 10. Pickett HA, Reddel RR. Molecular mechanisms of activity and derepression of alternative
605 lengthening of telomeres. Nat Struct Mol Biol. 2015;22(11):875-80. Epub 2015/11/20. doi:
606 10.1038/nsmb.3106

607 10.1038/nsmb.3106. Epub 2015 Nov 4. PubMed PMID: 26581522.
608 11. Bryan TM, Englezou A, Gupta J, Bacchetti S, Reddel RR. Telomere elongation in immortal
609 human cells without detectable telomerase activity. Embo J. 1995;14(17):4240-8. PubMed PMID:
610 7556065.
611 12. Yeager TR, Neumann AA, Englezou A, Huschtscha LI, Noble JR, Reddel RR. Telomerase-
612 negative immortalized human cells contain a novel type of promyelocytic leukemia (PML) body.
613 Cancer Research. 1999;59(17):4175-9. PubMed PMID: WOS:000082380200005.
614 13. Nabetani A, Yokoyama O, Ishikawa F. Localization of hRad9, hHus1, hRad1, and hRad17 and
615 caffeine-sensitive DNA replication at the alternative lengthening of telomeres-associated
616 promyelocytic leukemia body. J Biol Chem. 2004;279(24):25849-57. Epub 2004/04/13. doi:
617 10.1074/jbc.M312652200. PubMed PMID: 15075340.
618 14. Stavropoulos DJ, Bradshaw PS, Li X, Pasic I, Truong K, Ikura M, et al. The Bloom syndrome
619 helicase BLM interacts with TRF2 in ALT cells and promotes telomeric DNA synthesis. Hum Mol
620 Genet. 2002;11(25):3135-44. Epub 2002/11/22. doi: 10.1093/hmg/11.25.3135. PubMed PMID:
621 12444098.
622 15. Draskovic I, Arnoult N, Steiner V, Bacchetti S, Lomonte P, Londono-Vallejo A. Probing PML
623 body function in ALT cells reveals spatiotemporal requirements for telomere recombination. Proc
624 Natl Acad Sci U S A. 2009;106(37):15726-31. Epub 2009/09/01. doi: 10.1073/pnas.0907689106.
625 PubMed PMID: 19717459; PubMed Central PMCID: PMCPMC2747187.

626 16. Dunham MA, Neumann AA, Fasching CL, Reddel RR. Telomere maintenance by
627 recombination in human cells. Nat Genet. 2000;26(4):447-50. Epub 2000/12/02. doi:
628 10.1038/82586. PubMed PMID: 11101843.
629 17. Jiang WQ, Zhong ZH, Henson JD, Neumann AA, Chang AC, Reddel RR. Suppression of
630 alternative lengthening of telomeres by Sp100-mediated sequestration of the MRE11/RAD50/NBS1
631 complex. Mol Cell Biol. 2005;25(7):2708-21. Epub 2005/03/16. doi: 10.1128/MCB.25.7.2708-
632 2721.2005. PubMed PMID: 15767676; PubMed Central PMCID: PMCPMC1061646.
633 18. Cesare AJ, Reddel RR. Alternative lengthening of telomeres: models, mechanisms and
634 implications. Nat Rev Genet. 2010;11(5):319-30. Epub 2010/03/31. doi: 10.1038/nrg2763. PubMed
635 PMID: 20351727.
636 19. Zhang JM, Yadav T, Ouyang J, Lan L, Zou L. Alternative lengthening of telomeres through two
637 distinct break-induced replication pathways. Cell Rep. 2019;26(4):955-68.e3. Epub 2019/01/24. doi:
638 10.1016/j.celrep.2018.12.102

639 10.1016/j.celrep.2018.12.102. PubMed PMID: 30673617; PubMed Central PMCID:
640 PMCPMC6366628.
641 20. Lovejoy CA, Li W, Reisenweber S, Thongthip S, Bruno J, de Lange T, et al. Loss of ATRX,
642 genome instability, and an altered DNA damage response are hallmarks of the alternative
643 lengthening of telomeres pathway. PLoS Genet. 2012;8(7):e1002772. doi:
644 10.1371/journal.pgen.1002772. PubMed PMID: 22829774; PubMed Central PMCID: PMC3400581.
645 21. Heaphy CM, de Wilde RF, Jiao Y, Klein AP, Edil BH, Shi C, et al. Altered telomeres in tumors
646 with ATRX and DAXX mutations. Science. 2011;333(6041):425. PubMed PMID: 21719641.
647 22. Wong LH, McGhie JD, Sim M, Anderson MA, Ahn S, Hannan RD, et al. ATRX interacts with
648 H3.3 in maintaining telomere structural integrity in pluripotent embryonic stem cells. Genome Res.
649 2010;20(3):351-60. Epub 2010/01/30. doi: gr.101477.109 [pii]

650 10.1101/gr.101477.109. PubMed PMID: 20110566; PubMed Central PMCID: PMC2840985.
651 23. Goldberg AD, Banaszynski LA, Noh KM, Lewis PW, Elsaesser SJ, Stadler S, et al. Distinct
652 factors control histone variant H3.3 localization at specific genomic regions. Cell. 2010;140(5):678-
653 91. Epub 2010/03/10. doi: S0092-8674(10)00004-8 [pii]

654 10.1016/j.cell.2010.01.003. PubMed PMID: 20211137.
655 24. Ivanauskiene K, Delbarre E, McGhie JD, Kuntziger T, Wong LH, Collas P. The PML-associated
656 protein DEK regulates the balance of H3.3 loading on chromatin and is important for telomere
657 integrity. Genome Res. 2014;24(10):1584-94. doi: 10.1101/gr.173831.114. PubMed PMID:
658 25049225; PubMed Central PMCID: PMC4199371.
659 25. O'Sullivan RJ, Almouzni G. Assembly of telomeric chromatin to create ALTernative endings.
660 Trends Cell Biol. 2014;24(11):675-85. doi: 10.1016/j.tcb.2014.07.007. PubMed PMID: 25172551.
661 26. Episkopou H, Draskovic I, Van Beneden A, Tilman G, Mattiussi M, Gobin M, et al. Alternative
662 Lengthening of Telomeres is characterized by reduced compaction of telomeric chromatin. Nucleic
663 Acids Res. 2014;42(7):4391-405. Epub 2014/02/07. doi: 10.1093/nar/gku114

664 10.1093/nar/gku114. Epub 2014 Feb 5. PubMed PMID: 24500201; PubMed Central PMCID:
665 PMCPMC3985679.
666 27. Amorim JP, Santos G, Vinagre J, Soares P. The Role of ATRX in the Alternative Lengthening of
667 Telomeres (ALT) Phenotype. Genes (Basel). 2016;7(9). doi: 10.3390/genes7090066. PubMed PMID:
668 27657132; PubMed Central PMCID: PMCPMC5042396.
669 28. Bower K, Napier CE, Cole SL, Dagg RA, Lau LM, Duncan EL, et al. Loss of wild-type ATRX
670 expression in somatic cell hybrids segregates with activation of Alternative Lengthening of
671 Telomeres. PLoS One. 2012;7(11):e50062. Epub 2012/11/28. doi: 10.1371/journal.pone.0050062

672 10.1371/journal.pone.0050062. Epub 2012 Nov 20. PubMed PMID: 23185534; PubMed Central
673 PMCID: PMCPMC3502299.
674 29. Hu Y, Shi G, Zhang L, Li F, Jiang Y, Jiang S, et al. Switch telomerase to ALT mechanism by
675 inducing telomeric DNA damages and dysfunction of ATRX and DAXX. Sci Rep. 2016;6:32280. Epub

676 2016/09/01. doi: 10.1038/srep32280. PubMed PMID: 27578458; PubMed Central PMCID:
677 PMCPMC5006076.
678 30. Napier CE, Huschtscha LI, Harvey A, Bower K, Noble JR, Hendrickson EA, et al. ATRX
679 represses alternative lengthening of telomeres. Oncotarget. 2015;6(18):16543-58. PubMed PMID:
680 WOS:000359012000079.
681 31. Clynes D, Jelinska C, Xella B, Ayyub H, Scott C, Mitson M, et al. Suppression of the alternative
682 lengthening of telomere pathway by the chromatin remodelling factor ATRX. Nat Commun.
683 2015;6:7538. doi: 10.1038/ncomms8538. PubMed PMID: 26143912; PubMed Central PMCID:
684 PMC4501375.
685 32. Jacobs JP, Jones CM, Baille JP. Characteristics of a human diploid cell designated MRC-5.
686 Nature. 1970;227(5254):168-70. PubMed PMID: 4316953.
687 33. Jones RE, Oh S, Grimstead JW, Zimbric J, Roger L, Heppel NH, et al. Escape from Telomere-
688 Driven Crisis Is DNA Ligase III Dependent. Cell reports. 2014;8(4):1063-76. doi:
689 10.1016/j.celrep.2014.07.007. PubMed PMID: 25127141.
690 34. Sambrock J, Fritsch EF, Maniatis T. Molecular Cloning, A Laboratory Manual. Second ed.
691 New-York: Cold Spring Harbor Laboratory Press; 1989.
692 35. Capper R, Britt-Compton B, Tankimanova M, Rowson J, Letsolo B, Man S, et al. The nature of
693 telomere fusion and a definition of the critical telomere length in human cells. Genes Dev.
694 2007;21(19):2495-508. PubMed PMID: 17908935.
695 36. Britt-Compton B, Rowson J, Locke M, Mackenzie I, Kipling D, Baird DM. Structural stability
696 and chromosome-specific telomere length is governed by cis-acting determinants in humans. Human
697 Molecular Genetics. 2006;15(5):725-33. doi: 10.1093/hmg/ddi486. PubMed PMID:
698 WOS:000235432900006.
699 37. Henson JD, Cao Y, Huschtscha LI, Chang AC, Au AY, Pickett HA, et al. DNA C-circles are
700 specific and quantifiable markers of alternative-lengthening-of-telomeres activity. Nat Biotechnol.
701 2009;27(12):1181-5. Epub 2009/11/26. doi: 10.1038/nbt.1587. PubMed PMID: 19935656.
702 38. Mender I, Shay JW. Telomerase Repeated Amplification Protocol (TRAP). Bio Protoc.
703 2015;5(22). Epub 2016/05/18. doi: 10.21769/bioprotoc.1657

704 10.21769/bioprotoc.1657. PubMed PMID: 27182535; PubMed Central PMCID: PMCPMC4863463.
705 39. Cleal K, Jones RE, Grimstead JW, Hendrickson EA, Baird DM. Chromothripsis during telomere
706 crisis is independent of NHEJ and consistent with a replicative origin. Genome Res. 2019. Epub
707 2019/03/16. doi: 10.1101/gr.240705.118. PubMed PMID: 30872351.
708 40. Bond JA, Haughton MF, Rowson JM, Smith PJ, Gire V, Wynford-Thomas D, et al. Control of
709 replicative life span in human cells: barriers to clonal expansion intermediate between M1
710 senescence and M2 crisis. Mol Cell Biol. 1999;19(4):3103-14. PubMed PMID: 10082577.
711 41. Baird DM, Rowson J, Wynford-Thomas D, Kipling D. Extensive allelic variation and ultrashort
712 telomeres in senescent human cells. Nat Genet. 2003;33(2):203-7. PubMed PMID: 12539050.
713 42. Hahn WC, Stewart SA, Brooks MW, York SG, Eaton E, Kurachi A, et al. Inhibition of
714 telomerase limits the growth of human cancer cells. Nat Med. 1999;5(10):1164-70. PubMed PMID:
715 10502820.
716 43. Chang M, Arneric M, Lingner J. Telomerase repeat addition processivity is increased at
717 critically short telomeres in a Tel1-dependent manner in Saccharomyces cerevisiae. Genes Dev.
718 2007;21(19):2485-94. PubMed PMID: 17908934.
719 44. Allshire RC, Dempster M, Hastie ND. Human telomeres contain at least three types of G-rich
720 repeat distributed non-randomly. Nucleic Acids Res. 1989;17(12):4611-27. PubMed PMID: 2664709.
721 45. Baird DM, Jeffreys AJ, Royle NJ. Mechanisms underlying telomere repeat turnover, revealed
722 by hypervariable variant repeat distribution patterns in the human Xp/Yp telomere. Embo J.
723 1995;14(21):5433-43. PubMed PMID: 7489732.
724 46. Baird DM, Coleman J, Rosser ZH, Royle NJ. High levels of sequence polymorphism and
725 linkage disequilibrium at the telomere of 12q: implications for telomere biology and human
726 evolution. Am J Hum Genet. 2000;66(1):235-50. PubMed PMID: 10631154.
727 47. Min J, Wright WE, Shay JW. Alternative lengthening of telomeres can be maintained by
728 preferential elongation of lagging strands. Nucleic Acids Res. 452017. p. 2615-28.

729 48. Liddiard K, Ruis B, Takasugi T, Harvey A, Ashelford KE, Hendrickson EA, et al. Sister chromatid
730 telomere fusions, but not NHEJ-mediated inter-chromosomal telomere fusions, occur independently
731 of DNA ligases 3 and 4. Genome Res. 2016;26(5):588-600. doi: 10.1101/gr.200840.115. PubMed
732 PMID: 26941250; PubMed Central PMCID: PMCPMC4864465.
733 49. Lovejoy CA, Li W, Reisenweber S, Thongthip S, Bruno J, de Lange T, et al. Loss of ATRX,
734 genome instability, and an altered DNA damage response are hallmarks of the alternative
735 lengthening of telomeres pathway. PLoS Genet. 2012;8(7):e1002772. Epub 2012/07/26. doi:
736 10.1371/journal.pgen.1002772. PubMed PMID: 22829774; PubMed Central PMCID:
737 PMCPMC3400581.
738 50. Brosnan-Cashman JA, Yuan M, Graham MK, Rizzo AJ, Myers KM, Davis C, et al. ATRX loss
739 induces multiple hallmarks of the alternative lengthening of telomeres (ALT) phenotype in human
740 glioma cell lines in a cell line-specific manner. PLoS One. 2018;13(9):e0204159. Epub 2018/09/19.
741 doi: 10.1371/journal.pone.0204159

742 10.1371/journal.pone.0204159. eCollection 2018. PubMed PMID: 30226859; PubMed Central
743 PMCID: PMCPMC6143253.
744 51. O'Sullivan RJ, Arnoult N, Lackner DH, Oganesian L, Haggblom C, Corpet A, et al. Rapid
745 induction of alternative lengthening of telomeres by depletion of the histone chaperone ASF1. Nat
746 Struct Mol Biol. 2014;21(2):167-74. Epub 20140112. doi: 10.1038/nsmb.2754

747 10.1038/nsmb.2754. Epub 2014 Jan 12. PubMed PMID: 24413054; PubMed Central PMCID:
748 PMCPMC3946341.
749 52. Leung JW, Ghosal G, Wang W, Shen X, Wang J, Li L, et al. Alpha thalassemia/mental
750 retardation syndrome X-linked gene product ATRX is required for proper replication restart and
751 cellular resistance to replication stress. J Biol Chem. 2013;288(9):6342-50. Epub 20130116. doi:
752 10.1074/jbc.M112.411603. PubMed PMID: 23329831; PubMed Central PMCID: PMCPMC3585069.
753 53. Huh MS, Ivanochko D, Hashem LE, Curtin M, Delorme M, Goodall E, et al. Stalled replication
754 forks within heterochromatin require ATRX for protection. Cell Death & Disease. 2016;7(5):e2220-e.
755 doi: 10.1038/cddis.2016.121.
756 54. Wang Y, Yang J, Wild AT, Wu WH, Shah R, Danussi C, et al. G-quadruplex DNA drives genomic
757 instability and represents a targetable molecular abnormality in ATRX-deficient malignant glioma.
758 Nat Commun. 2019;10(1):943. Epub 2019/02/28. doi: 10.1038/s41467-019-08905-8. PubMed PMID:
759 30808951; PubMed Central PMCID: PMCPMC6391399.
760 55. Watson LA, Solomon LA, Li JR, Jiang Y, Edwards M, Shin-ya K, et al. Atrx deficiency induces
761 telomere dysfunction, endocrine defects, and reduced life span. J Clin Invest. 2013;123(5):2049-63.
762 Epub 20130408. doi: 10.1172/jci65634. PubMed PMID: 23563309; PubMed Central PMCID:
763 PMCPMC3635723.
764 56. Ait Saada A, Lambert SAE, Carr AM. Preserving replication fork integrity and competence via
765 the homologous recombination pathway. DNA Repair (Amst). 2018;71:135-47. Epub 2018/09/18.
766 doi: 10.1016/j.dnarep.2018.08.017

767 10.1016/j.dnarep.2018.08.017. Epub 2018 Aug 25. PubMed PMID: 30220600; PubMed Central
768 PMCID: PMCPMC6219450.
769 57. Zhang JM, Genois MM, Ouyang J, Lan L, Zou L. Alternative lengthening of telomeres is a self-
770 perpetuating process in ALT-associated PML bodies. Mol Cell. 2021;81(5):1027-42.e4. Epub
771 2021/01/17. doi: 10.1016/j.molcel.2020.12.030

772 10.1016/j.molcel.2020.12.030. Epub 2021 Jan 15. PubMed PMID: 33453166.
773 58. Abid HZ, McCaffrey J, Raseley K, Young E, Lassahn K, Varapula D, et al. Single-molecule
774 analysis of subtelomeres and telomeres in Alternative Lengthening of Telomeres (ALT) cells. BMC
775 Genomics. 2020;21(1):485. Epub 20200715. doi: 10.1186/s12864-020-06901-7

776 10.1186/s12864-020-06901-7. PubMed PMID: 32669102; PubMed Central PMCID:
777 PMCPMC7364475.

778 59. Seo B, Kim C, Hills M, Sung S, Kim H, Kim E, et al. Telomere maintenance through
779 recruitment of internal genomic regions. Nat Commun. 2015;6:8189. Epub 2015/09/19. doi:
780 10.1038/ncomms9189

781 10.1038/ncomms9189. PubMed PMID: 26382656; PubMed Central PMCID: PMCPMC4595603.
782 60. Teng SC, Chang J, McCowan B, Zakian VA. Telomerase-independent lengthening of yeast
783 telomeres occurs by an abrupt Rad50p-dependent, Rif-inhibited recombinational process. Molecular
784 Cell. 2000;6(4):947-52. doi: 10.1016/s1097-2765(05)00094-8. PubMed PMID:
785 WOS:000090136700018.
786 61. Varley H, Pickett HA, Foxon JL, Reddel RR, Royle NJ. Molecular characterization of inter-
787 telomere and intra-telomere mutations in human ALT cells. Nat Genet. 2002;30(3):301-5. PubMed
788 PMID: 11919561.
789 62. Kockler ZW, Comeron JM, Malkova A. A unified alternative telomere-lengthening pathway in
790 yeast survivor cells. Mol Cell. 2021. Epub 2021/02/28. doi: 10.1016/j.molcel.2021.02.004. PubMed
791 PMID: 33639094.
792 63. Lee M, Hills M, Conomos D, Stutz MD, Dagg RA, Lau LM, et al. Telomere extension by
793 telomerase and ALT generates variant repeats by mechanistically distinct processes. Nucleic Acids
794 Res. 2014;42(3):1733-46. Epub 2013/11/15. doi: 10.1093/nar/gkt1117

795 10.1093/nar/gkt1117. Epub 2013 Nov 12. PubMed PMID: 24225324; PubMed Central PMCID:
796 PMCPMC3919612.
797 64. Lee M, Teber ET, Holmes O, Nones K, Patch AM, Dagg RA, et al. Telomere sequence content
798 can be used to determine ALT activity in tumours. Nucleic Acids Res. 2018;46(10):4903-18. Epub
799 2018/05/03. doi: 10.1093/nar/gky297. PubMed PMID: 29718321; PubMed Central PMCID:
800 PMCPMC6007693.
801 65. Conomos D, Stutz MD, Hills M, Neumann AA, Bryan TM, Reddel RR, et al. Variant repeats are
802 interspersed throughout the telomeres and recruit nuclear receptors in ALT cells. J Cell Biol.
803 2012;199(6):893-906. Epub 2012/12/12. doi: 10.1083/jcb.201207189

804 10.1083/jcb.201207189. PubMed PMID: 23229897; PubMed Central PMCID: PMCPMC3518223.

805

806 **Figure Legends**

807 **Fig 1: ALT upregulation and maintenance in the absence of ATRX in primary fibroblasts undergoing**
808 **a telomere-driven "crisis".** Growth curves displaying PDs graphed against days in culture for (A)
809 HCA2^{HPVE6E7} clones (n = 6) that failed to escape crisis and (B) HCA2^{HPVE6E7} clones (n = 6) that successfully
810 escaped crisis. (C) Western blots displaying ATRX protein expression in "no escape" and "escape"
811 clones with vinculin expression used as a loading control. (D) Quantification of the ATRX protein
812 expression using the ATRX:vinculin ratio normalised to the parental cell line expressed in arbitrary
813 units (AU) with the standard deviation (SD) used as error bars and the clone number displayed across
814 the bottom. STELA profiles at the XpYp and 17p chromosome ends for (E) clone 1 that failed to escape
815 crisis and (F) clone 37 that successfully escaped crisis; with the PD indicated across the top and the
816 mean telomere length in kb, also represented as orange dotted lines on the blot, and SD across the
817 bottom. (G) C-circle assay slot blots with (+ pol) and without (- pol) polymerase samples with the PD
818 and clone number stated across the bottom.

819

820 **Fig 2: ALT-like initiation in the absence of ATRX in HCT116 epithelial cancer cells undergoing a**
821 **telomere-driven "crisis".** (A) Growth curves displaying PDs versus days in culture for the 149
822 HCT116$^{ATRX-/0:DN-hTERT}$ single cell clones picked across four DN-hTERT transfections represented by the
823 four separate panels; green clones that presented ALT-like telomere elongation; blue clones are
824 telomerase-positive escapees; red clones showed ALT-like characteristics, but did not survive; and
825 black clones are clones that did not survive. STELA profiles at the (B) 17p and (C) XpYp chromosome
826 ends for the HCT116$^{ATRX-/o}$ parental; HCT116$^{ATRX-/o:DN-hTERT}$ clones 1 and 8 that did not survive and clones
827 2, 3 and 4 that exhibited an ALT-like elongation event; and HCT116$^{ATRX-/o:Puro}$ clone as a transfection
828 control with the PD indicated across the top and the mean telomere length alongside the elongated
829 allele mean in kb shown across the bottom; also represented as orange and red dotted lines,
830 respectively, on the blots.

831

832 **Fig 3: ALT-like telomere elongation and long-term telomerase upregulation in HCT116 epithelial**
833 **cells.** (A) STELA profiles at the 17p chromosome end for the HCT116$^{ATRX-/o}$ parental; HCT116$^{ATRX-/o:DN-}$
834 ^{hTERT} ALT-like clones 2, 3 and 4; and HCT116$^{ATRX-/o:Puro}$ with PD points indicated above and the overall
835 mean telomere length in black (represented as orange dotted lines on the blot) displayed below
836 together with allelic mean telomere lengths (red and green) also represented as dotted lines on the
837 blot. The rate of erosion is represented by ΔTel and is expressed in bp/PD. (B) Quantification of
838 telomerase activity (expressed in total product generated: TPG) on the left axis and the C-circle
839 intensity (expressed in arbitrary units: AU) on the right axis. SD was used as error bars and the PD is
840 indicated on the X-axis. (C) C-circle assay slot blots with (+ pol) and without (- pol) polymerase samples
841 with the PD and clone number shown across the bottom. Striped bars indicate telomerase activity and
842 solid bars C-circles.

843

844 **Fig 4: Chromosome specific elongation of short telomeres upon ALT upregulation in HCT116**
845 **epithelial cells.** STELA profiles at the (A) 5p, (B) 7q, (C) 9p and (D) 8q chromosome ends for HCT116^{ATRX-}
846 $^{/o:DN-hTERT}$ ALT-like clone 3 alongside the HCT116$^{ATRX-/o}$ parental clone at the 8q chromosome end for
847 reference with the PD indicated across the top and the mean telomere length indicated in kb across
848 the bottom and also represented as orange dotted lines on the blot.

849

850 **Fig 5: ALT elongation arises from multiple independent events.** Examples of telomere sequences
851 obtained from PacBio sequencing of STELA amplicons obtained from HCT116$^{ATRX-/o}$ and HCA2$^{HPVE6E7;ATRX-}$
852 $^{/o}$ cells at the XpYp, 17p and 7q chromosome ends prior to crisis (Parental) and a single clone of each
853 exhibiting characteristics of ALT post crisis, denoted as ALT from HCA2$^{HPVE6E7;ATRX-/o}$ fibroblasts and ALT-
854 L (ALT-like) from HCT116$^{ATRX-/o}$. Each telomeric allele is displayed separately with the parental (PAR)
855 telomeric allele above and the derived ALT allele (ALT) below. The red bar displayed above the
856 parental allele sequences indicates distinct TVR patterns conserved in ALT alleles. The telomere and 6

857 nt TVR sequences are coded as follows: ■ TTAGGG; ■ TCAGGG; ■ TTCGGG; ■ GTAGGG; ■ TGAGGG; ■

858 TTGGGG; ■ TAAGGG; ■ CTAGGG; ■ TTTGGG; ■ AGAGGG; □ TVRs ≤ 6 nt.

859

860 **Supplementary figure legends**

861 **S1 Fig: ALT activation and maintenance in the absence of ATRX in MRC5 primary fibroblasts**

862 **undergoing a telomere-driven "crisis".** Growth curves displaying population doublings (PDs) against

863 days in culture for (A) MRC5^{HPVE6E7} clones (n = 5) that failed to escape crisis and (B) MRC5^{HPVE6E7} clones

864 (n = 9) that successfully escaped crisis. (C) Western blots displaying ATRX protein expression in "no

865 escape" and "escape" clones with Vinculin expression used as loading control. STELA profiles (overall

866 and GC or AT allele-specific) at the XpYp chromosome end for clone 1 (D) that failed to escape crisis

867 and clone 121 (E) that successfully escaped crisis; with the PD points stated across the top and the

868 mean of the telomere length distributions detailed across the bottom, with the mean also represented

869 as orange dotted lines on the blot. (F) C-circle assay slot blots of the with (+ pol) and without (- pol)

870 ϕ29 DNA polymerase samples with the PD and clone number stated across the bottom.

871

872 **S2 Fig: Sequence verification of selected clones exposed to ATRX CRISPR.** Examples of three

873 HCA2^{HPVE6E7} clones that presented a mutated ATRX gene upon screening that were subsequently

874 analysed by sequencing. In yellow is indicated the CRISPR target site as well as a Sml1 restriction site;

875 dashes represent deletions.

876

877 **S3 Fig: Induction of a telomere-driven crisis upon transfection of E6E7 viral oncoproteins in**

878 **fibroblasts WT for ATRX.** Growth curves displaying population doublings (PDs) against days in culture

879 of the 6 HCA2^{HPVE6E7} single cell clones.

880

881 **S4 Fig: Homogeneous telomere length distributions in control and no escape clones**. STELA profiles
882 at the XpYp and 17p chromosome ends in HCA2^{HPVE6E7} cells for (A) clones 1 and 4 used as controls and
883 (B) clones 2 and 44 that failed to escape crisis; with the PD points stated across the top and the mean
884 of the telomere length distributions detailed across the bottom, with the mean also represented as
885 orange dotted lines on the blot.

886

887 **S5 Fig: Heterogeneous telomere length distributions upon loss of ATRX and escape from crisis**. STELA
888 profiles for (A) HCA2$^{HPVE6E7\ ATRX-/-}$ clones 18 and 21 at the XpYp and 17p chromosome end; and (B)
889 MRC5$^{HPVE6E7\ ATRX-/-}$ clones 9 and 46 at the XpYp chromosome end for the combined alleles as well as for
890 specific (GC or AT as indicated above) alleles; with the PD points stated across the top and the mean
891 and standard deviation of the telomere length distributions detailed across the bottom, with the mean
892 also represented as orange dotted lines on the blot.

893

894 **S6 Fig: Fusion profiles reveal an increase of end-to-end fusions in escapees during crisis.** A) Example
895 of fusion profiles for clone 1 (no escape) and clone 21 (escape) across multiple PD points (detailed
896 across the top) and U2OS as an ALT-positive control. Blots were serially Southern hybridised with the
897 telomere-adjacent DNA probes indicated on the left and the number of unique fusions stated below
898 the blots. B) Bar charts depicting the number of XpYp (purple), 17p (white), 21q (grey) and total (black)
899 fusion events as escapees are transiting through crisis and immortalising. (Number of diploid genome
900 equivalents analysed = 2×10^4).

901

902 **S7 Fig:** Quantification of the C-circle slot blot intensity by subtracting the background (-pol) to the +pol
903 sample and normalised to the HCA2$^{HPVE6E7;ATRX-/o}$ fibroblasts parental cell line expressed in arbitrary
904 unit (AU). The PD and clone number are stated across the bottom.

905

906 **S8 Fig: An absence of detectable telomerase activity in fibroblast cells that escaped crisis in the**
907 **absence of ATRX.** TRAP assay results at the indicated PD points after the escape from crisis in A)
908 HCA2$^{HPVE6E7\ ATRX-/-}$ cells and B) MRC5$^{HPVE6E7\ ATRX-/-}$ cells with the WT HCT116 cell line used as a positive
909 control.

910

911 **S9 Fig: Crisis induces visible phenotypic changes to cells.** 4X magnification of HCT116$^{ATRX-/-:DN-hTERT}$ cells
912 (A) prior to crisis where they display small and healthy morphologies; and (B) large and multi-
913 nucleated cells characteristic of cells undergoing crisis.

914

915 **S10 Fig: Cell growth of puromycin control HCT116$^{ATRX-/-}$ clones.** Growth curve displaying PDs against
916 days in culture for the puromycin control clones (n = 12) that were transfected with a puromycin
917 selection gene to query the effects of a viral integration on HCT116$^{ATRX-/-}$ cells survival.

918

919 **S11 Fig: ALT-like elongation does not occur at all short telomeres.** STELA profiles at the XpYp and 17p
920 chromosome ends for HCT116$^{ATRX-/-:DN-hTERT}$ clone 147 that underwent telomere elongation at the XpYp
921 chromosome end, but not at 17p, despite achieving replicative immortality. PD points are detailed
922 across the top and the overall mean telomere length in black (represented by orange dotted lines on
923 the blot) together with the estimated allelic telomere length distributions (red and green) across the
924 bottom, also represented as dotted lines on the blot.

925

926 **S12 Fig: Telomeric elongation during crisis is allele specific.** 17p STELA of sub-clonal populations from
927 Clone 3 (PD31) that successfully escaped crisis following ALT-like elongation of short telomeres. PD
928 points from the point of single-cell cloning are indicated above, with the allele-specific mean telomere
929 length detailed below. Sub-clone 2 highlighted in red died at PD17. Sub-clone 11 was serially passaged
930 in culture, Δ telomere allelic telomere lengths are detailed below.

931

932 **S13 Fig: Telomere erosion following the expression of DN-hTERT in HCT116$^{ATRX-/-:DN-hTERT}$ clones.**
933 STELA profiles at the (A) 17p and (B) XpYp chromosome ends with the PD stated across the top and
934 the overall mean telomere length in black (represented as orange dotted lines on the blot), the longer
935 allele in green, the shorter allele in red across the bottom also represented as dotted lines on the blot.
936 The rate of erosion is represented by ΔTel in bp/PD. (C) Scatter plot depicting the mean telomere
937 length of all available samples at the first sampling point and last sampling points for the 17p and XpYp
938 chromosome ends with the p value stated above derived from a Mann-Whitney test (p-value < 0.05,
939 highlighted in red).

940

941 **S14 Fig: Increased heterogeneity of telomere length distributions upon the escape from crisis in**
942 **HCT116$^{ATRX-/-:DN-hTERT}$ clones.** STELA profiles at the (A) XpYp and (B) 17p chromosome ends for clones
943 92 and 111 which successfully escaped crisis activity with the PD stated across the top and the overall
944 mean telomere length and standard deviation in black (represented by orange dotted lines on the
945 blot), the longer allele in green, the shorter allele in red across the bottom also represented as dotted
946 lines on the blot. (C) Scatter plot depicting the standard deviation for all available escaping clones
947 before (black circles) and after crisis (black triangles) or after crisis only if no pre-crisis sample was
948 available (red triangles) at the XpYp and 17p chromosome ends. The p-value stated above were
949 derived from a student's t-test (p-value < 0.05, highlighted in red).

950

951 **S15 Fig: Consistent ALT-like telomere elongation at the XpYp chromosome end in HCT116$^{ATRX-/-:DN-}$**
952 **^{hTERT} clones following the escape from crisis**. STELA profiles at the XpYp chromosome end for the
953 HCT116$^{ATRX-/-}$ parental and the HCT116$^{ATRX-/-:DN-hTERT}$ ALT-like clones 2, 3 and 4 with the PD stated across
954 the top and the mean telomere length in black (represented as orange dotted lines on the blot) and
955 the allele that underwent telomere extension in red across the bottom also represented as dotted
956 lines on the blot. The rate of erosion is represented by ΔTel in bp/PD.

957

958 **S16 Fig: C-circles detected in the absence of telomeric elongation in HCT116$^{ATRX-/-:DN-hTERT}$ clones that**
959 **escaped crisis.** (A) C-circle assay slot blots with (+ pol) and without (- pol) polymerase with the PD and
960 clone number stated across the bottom. (B) Quantification of the slot blot intensity by subtracting the
961 background (-pol) to the +pol sample and normalised to the HCT116$^{ATRX-/-}$ parental cell line expressed
962 in arbitrary unit (AU) with the standard deviation used as error bars. The PD and clone number are
963 stated across the bottom. (C) STELA profiles at the XpYp chromosome end with the PD across the top
964 and the mean telomere length across the bottom also represented as orange dotted lines on the blot.
965 (D) Telomerase activity quantification expressed in total product generated (TPG) with the standard
966 deviation used as error bars where possible.

967

968 **S17 Fig: ALT-like activity does not always confer replicative immortality.** STELA profiles at (A) XpYp
969 and (B) 17p chromosome ends for HCT116$^{ATRX-/-:DN-hTERT}$ clones 108 and 132, which underwent an ALT-
970 like elongation at XpYp, but failed to escape crisis. PD is detailed across the top; the mean telomere
971 length in black (represented as orange dotted lines on the blot), the shorter allele prior to crisis in red
972 and the longer allele prior to crisis in green across the bottom also represented as dotted lines on the
973 blot. (C) C-circle assay slot blots with (+ pol) and without (- pol) polymerase samples with the PD and
974 clone number stated across the bottom. (D) Quantification of C-circle intensity by subtracting the
975 background (-pol) to the +pol sample normalised to the HCT116$^{ATRX-/-}$ parental expressed in arbitrary
976 unit (AU) with the standard deviation used as error bars. The PD and clone number is stated across
977 the bottom.

978

979 **S18 Fig: Consistent chromosome-specific elongation of telomeres.** STELA profiles at the 5p, 7q, 9p
980 and 8q chromosome ends for HCT116$^{ATRX-/-:DN-hTERT}$ (A) clone 2 and (B) clone 4 with the PD across the
981 top and the mean telomere length across the bottom also represented as orange dotted lines on the
982 blot. (C) Scatter plot displaying the elongated telomere distributions at the XpYp, 17p, 7q, 5p and 9p

983 chromosome ends of the three clones that successfully escaped crisis using the ALT mechanism with
984 standard deviation used as error bars. (D) Scatter plot displaying the insertion lengths (mean telomere
985 length post-elongation minus the mean telomere length prior to crisis) at the XpYp, 17p, 7q, 5p and
986 9p chromosome ends.

987

988 **S19 Fig: Altered telomere variant repeat patterns in ALT-positive clones.** The total proportion of
989 specific variant repeats combining all reads expressed in percentage (calculated by combining and
990 averaging the number of a specific variant normalised to the telomere length) for the parental and
991 the ALT clone with corresponding bar charts expressing the fold change in variant repeat proportion
992 when comparing parental and ALT clone using a log scale (with the score of 1 representing no change)
993 for (A) HCT116 model; (B) HCA2 model; and (C) U2OS.

994

995 **S20 Fig: Insertion of TVRs is cell line specific and arises from multiple events.** Examples of telomere
996 sequences obtained from PacBio sequencing of STELA amplicons obtained from HCT116$^{ATRX-/o}$ and
997 HCA2$^{HPVE6E7;ATRX-/o}$ cells at the XpYp, 17p and 7q chromosome ends prior to crisis (Parental) and a single
998 clone of each exhibiting characteristics of ALT post crisis, denoted as ALT from HCA2$^{HPVE6E7;ATRX-/o}$
999 fibroblasts and ALT-L (ALT-like) from HCT116$^{ATRX-/o}$ and ALT positive U2OS cells. Telomere and 6 nt
1000 variant repeat sequences are coded as follows: ■ TTAGGG; ■ TCAGGG; ■ TTCGGG; ■ GTAGGG; ■
1001 TGAGGG; ■ TTGGGG; ■ TAAGGG; ■ CTAGGG; ■ TTTGGG; ■ AGAGGG; ■ TVRs ≤ 6 nt.

1002

1003 **S21 Fig: Increased rate of structural variants in telomerase escapees but not in cells exhibiting ALT-**
1004 **like characteristics.** A) Structural variant counts for ALT-surviving, ALT-died and telomerase-positive
1005 clones with the P value as determined by a Mann-Whitney test stated above. Statistical difference
1006 highlighted in red (P value < 0.05). Clones and timepoints at which telomerase was active are
1007 highlighted in orange. B) Complex rearrangements on chromosomes 3 and 13 in ALT-like clone 147.

1008 **S1 Table. Summarising data from HCT116 clones**.

1009 **S1 Methods.** Supplementary methods describing PacBio SMRT sequencing analysis data processing

1010 and telomere variant repeat analysis.

1011 **Figure 1**

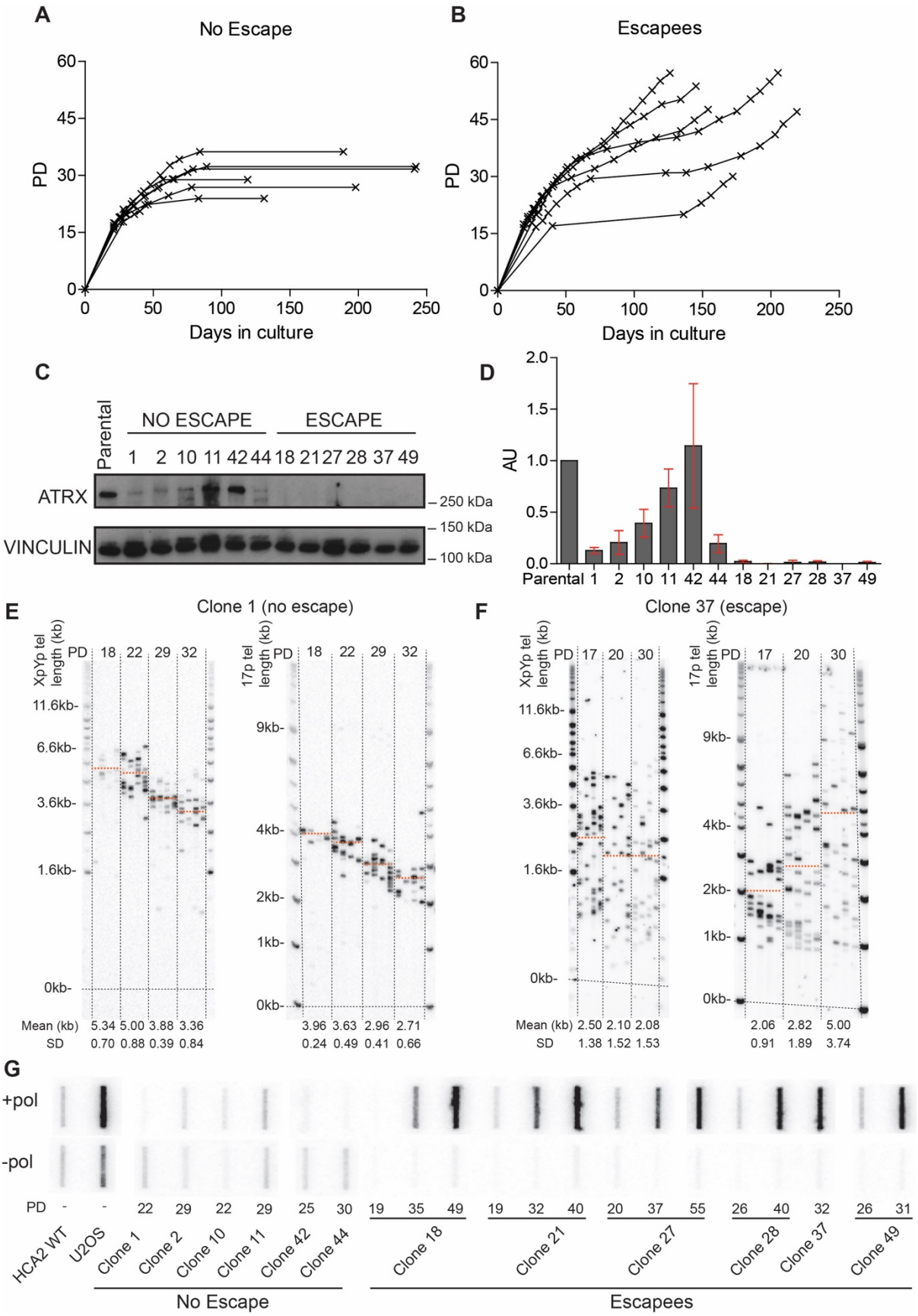

1012

1013

1014 **Figure 2**

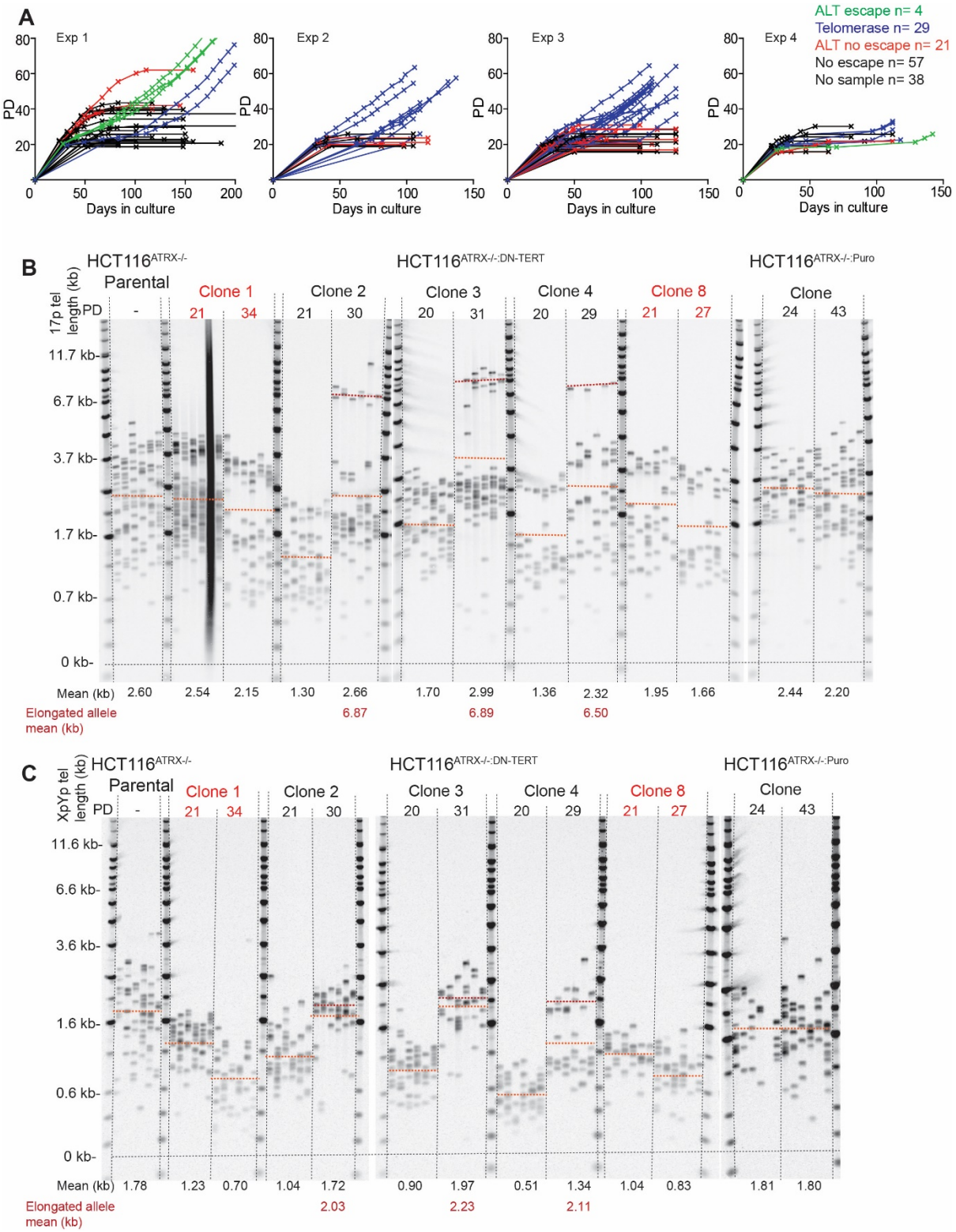

1015

1016

1017 **Figure 3**

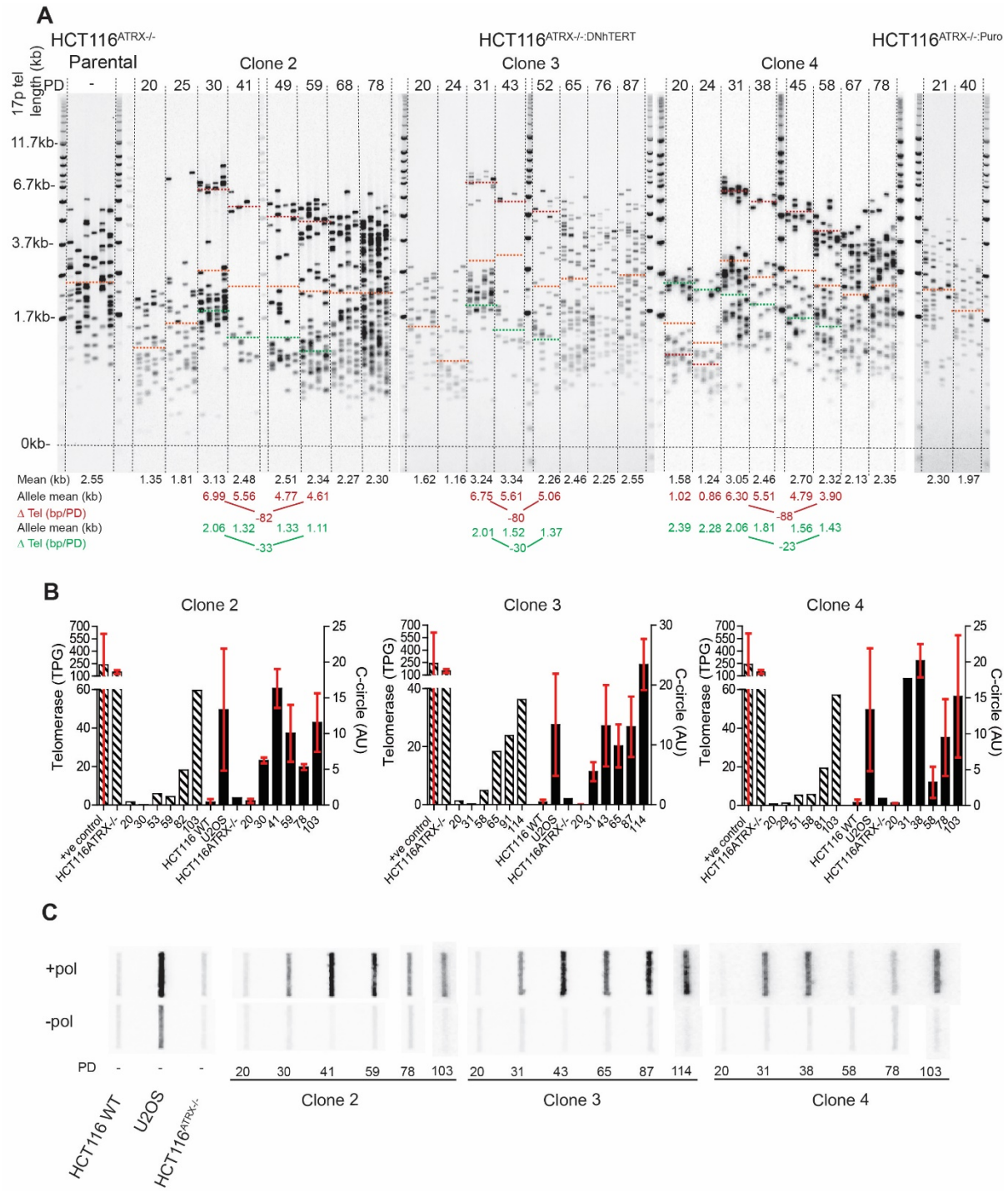

1018

1019

1020 **Figure 4**

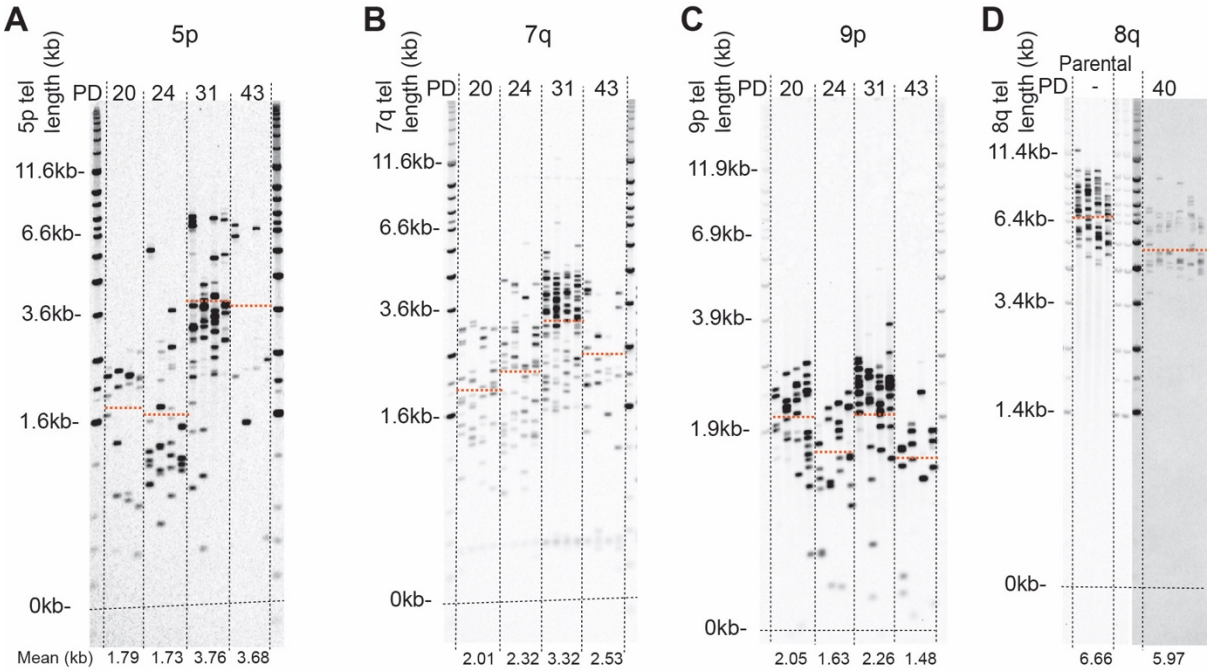

1021

1022

Figure 5

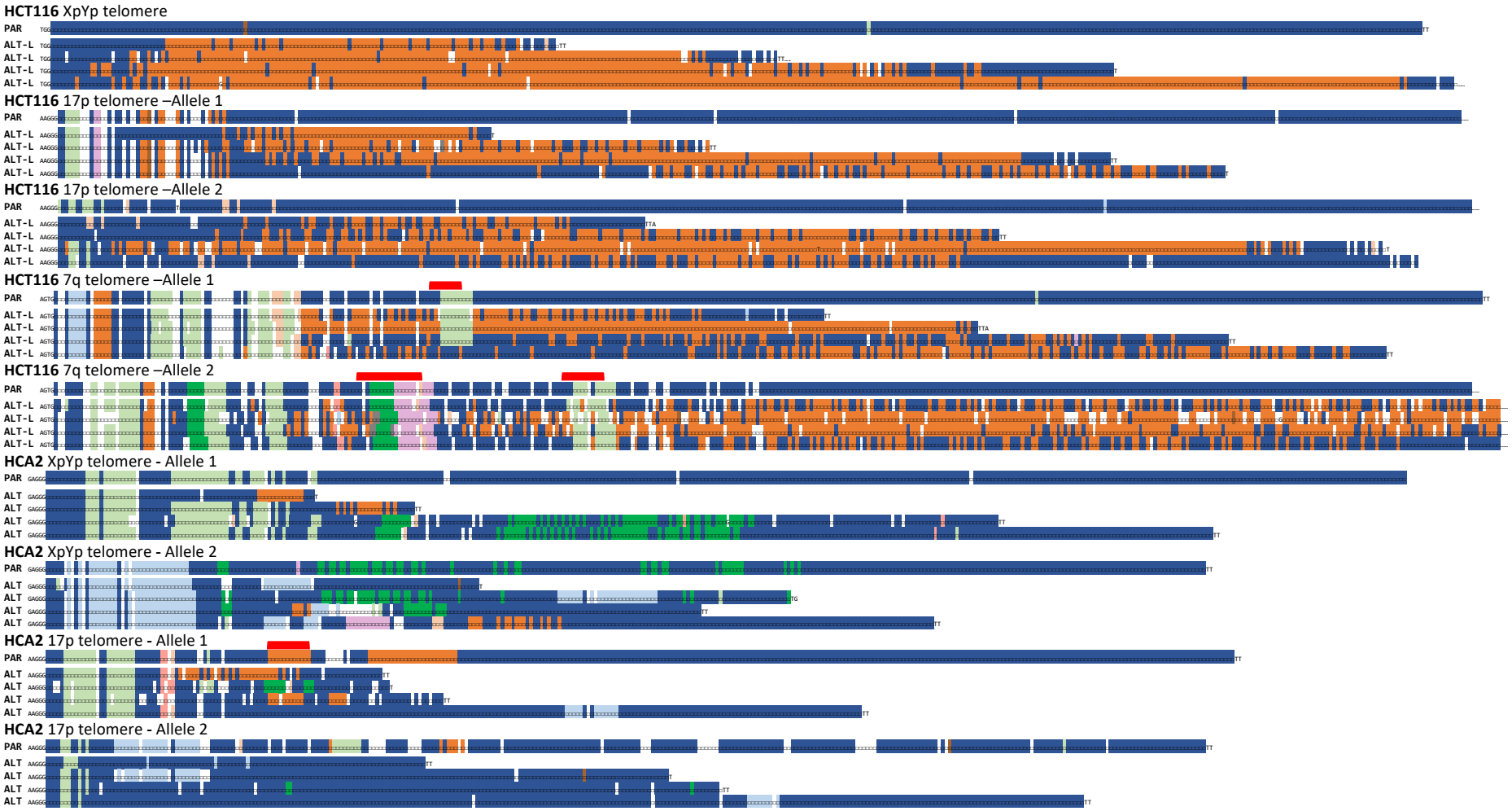
HCT116 XpYp telomere
PAR
ALT-L
ALT-L
ALT-L
ALT-L
HCT116 17p telomere –Allele 1
PAR
ALT-L
ALT-L
ALT-L
ALT-L
HCT116 17p telomere –Allele 2
PAR
ALT-L
ALT-L
ALT-L
ALT-L
HCT116 7q telomere –Allele 1
PAR
ALT-L
ALT-L
ALT-L
ALT-L
HCT116 7q telomere –Allele 2
PAR
ALT-L
ALT-L
ALT-L
ALT-L
HCA2 XpYp telomere - Allele 1
PAR
ALT
ALT
ALT
ALT
HCA2 XpYp telomere - Allele 2
PAR
ALT
ALT
ALT
ALT
HCA2 17p telomere - Allele 1
PAR
ALT
ALT
ALT
ALT
HCA2 17p telomere - Allele 2
PAR
ALT
ALT
ALT
ALT